Chapter 4

RESULTS

4.1 Effect of carbon and nitrogen source

Both the highest mycelial growth with maximum afp production were observed with soluble starch **(Table 4.1)** among all the five carbon sources investigated. Different carbon sources might have different effects of catabolic repression on the cellular secondary metabolism. The specific growth rates (μ) and specific rate of product formation (Q_P) in the soluble starch medium was 0.012 h^{-1} and 0.0026 mg $gdcw^{-1}$ h^{-1}, respectively.

Table 4.1 Effect of different carbon sources on mycelial growth and afp production by *A. giganteus* MTCC 8408 in basal Olson media **[78]** under submerged fermentation.

Carbohydrates (2%, w/v)	Specific growth rate (μ, h^{-1})	Cell biomass ($gdcw\,L^{-1}$)	Afp (mg L^{-1})	Final pH	$Q_p=Y_{p/x}\times\mu$ (mg $gdcw^{-1}$ h^{-1})
Glucose	0.007	21.48±0.15	2.75±0.05	5.66±0.03	0.0009
Maltose	0.003	22.92±0.23	3.69±0.11	5.21±0.09	0.0004
Lactose	0.009	23.74±0.18	4.87±0.08	5.88±0.11	0.0018
Sucrose	0.010	21.6±0.28	2.8±0.18	5.34±0.10	0.0013
Soluble starch	0.012	24.69±0.19	5.42±0.11	5.78±0.05	0.0026

Shifting from glucose to soluble starch supplemented caused a shift from a pelleted form to dispersed, `pulp-like' growth with consequent increase in afp production. Keeping this view, preliminary investigations were made to understand the role of various macro-nutrients level required for afp production which had significant morphological impact in submerge fermentation.

In glucose and maltose, fungal cell grew as hollow mycelial pellets (induced high mass transfer limitation) whereas in soluble starch and lactose, it grew as dispersed phase pulp like growth (induced high mass transfer coefficient).

Among the various nitrogen sources examined, both the maximum mycelial growth and afp production was achieved with corn steep liquor (CSL) and proteose peptone **(Table 4.2).**

Table 4.2 Effect of nitrogen sources on mycelial growth and afp production by *A. giganteus* MTCC 8408 in basal Olson media using soluble starch as carbon source under submerge fermentation.

Nitrogen (3%)	Cell biomass	Afp (mg L^{-1})	Final pH
Organic nitrogen:	(gdcw L^{-1})		
Peptone	21.66±0.11	2.15±0.05	5.25±0.15
Beef extract	23.58±0.09	2.85±0.11	5.50±0.14
CSL	24.21±0.18	5.66±0.09	5.66±0.03
Proteose peptone	23.78±0.12	4.12±0.12	5.18±0.11
CSL (2%) + Proteose peptone (1%)	28.75±0.10	9.98±0.15	6.02±0.05
Beef extract (2%) + peptone (1%)	24.88±0.18	7.98±0.06	6.40±0.09
Inorganic Nitrogen:			
Ammonium nitrate	10.56±0.23	1.98±0.06	4.74±0.08
Ammonium citrate	5.23 ±0.11	4.67±0.06	3.42±0.11
Ammonium chloride	3.88±0.14	3.56±0.12	3.88±0.02
Sodium nitrate	5.46±0.19	1.11±0.11	5.47±0.05

Antifungal protein production was proportionally increased and reached maximum at 20 g L^{-1} soluble starch concentration within the ranges 10 g L^{-1} to 50 g L^{-1}, while the maximum mycelial growth was achieved at 30 g L^{-1} **(Figure 4.1a).** Among the seven different nitrogen sources examined, both the maximum mycelial growth and afp production was achieved at 30 g L^{-1} when 2% corn steep liquor (CSL) with 1% proteose peptone was employed as nitrogen source **(Figure 4.1b).**

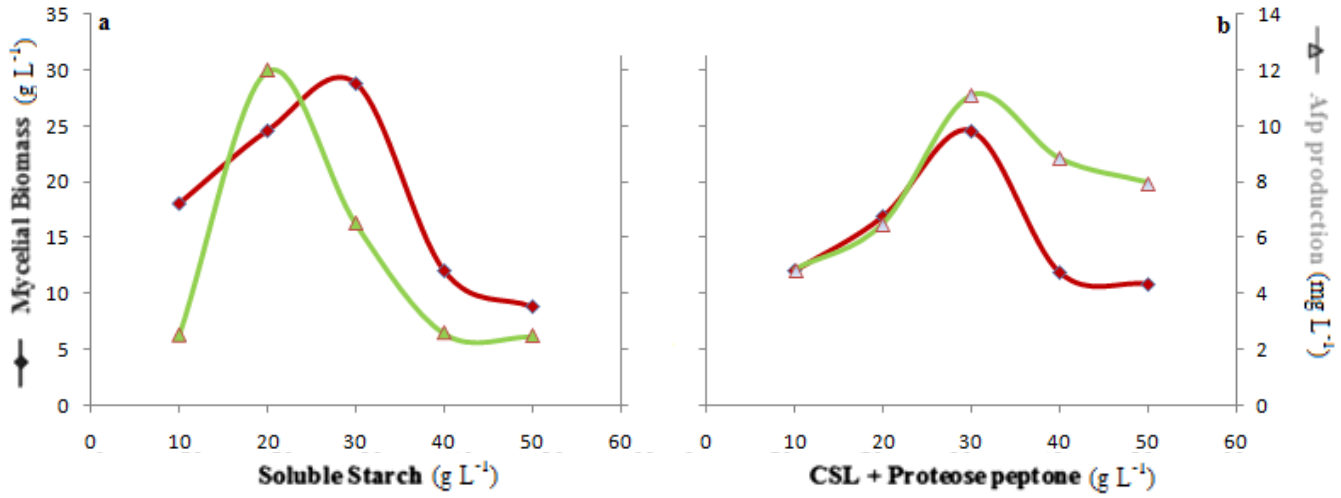

Figure 4.1 Effect of soluble starch and CSL with proteose peptone under varying concentration on **(a)** mycelial growth and **(b)** afp production in batch culture under submerged fermentation by *A. giganteus* MTCC 8408.

4.2 Effect of pH and temperature

The present study revealed that physical factor, pH and temperature were vital for afp production. Both maximum mycelial biomass growth and afp yield were observed at 25^0C **(Figure 4.2),** which is comparable to many kinds of ascomycetes that have relatively low temperature optima in their submerged cultures.

It was noteworthy that fermentation system can have a significant impact on the industrial application because of low material cost of carbon and nitrogen sources.

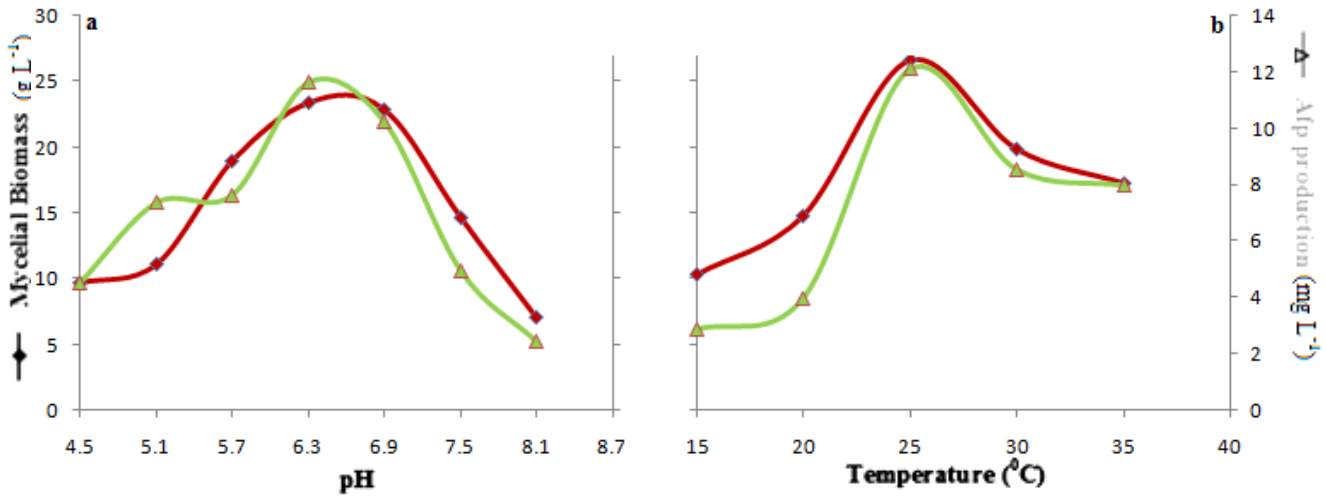

Figure 4.2 Effect of initial pH and temperature on **(a)** mycelial growth and **(b)** afp production in modified Olson media under submerged fermentation by *A. giganteus* MTCC 8408.

4.3 Effect of slant age and inoculum volume

Amongst several physiological properties, the slant age and inoculum volume (% v/v) may play an important role in fungal development. As shown in **Table 4.3**, the slant age and inoculum volume appeared to have little or no obvious effect on the mycelial biomass growth but have profound effect on afp production.

Table 4.3 Effect of slant age and inoculum level on mycelial growth and afp production by *A. giganteus* MTCC 8408 in modified Olson media under submerge fermentation

Slant age (day)	Inoculum volume (% v/v)	Afp (mg L^{-1})	Cell biomass (gdcw L^{-1})
3	2.5	2.98	13.9
7	2.5	1.78	15.8
11	2.5	5.53	15.1
3	5.0	6.11	21.7
7	5.0	9.98	24.2
11	5.0	5.53	23.2
3	10	5.98	24.8
7	10	3.84	28.9
11	10	2.77	23.7

4.4 Effect of C/N ratio and microelements (Taguchi DOE L_8 OA)

Based on the results of OFAT approach, the suitable carbon and nitrogen sources were soluble starch and CSL with proteose peptone, respectively. The upper and lower limits of these two variable were chosen as soluble starch (2%): 40 g L^{-1}; 60 g L^{-1} and CSL (2%) with proteose peptone (1%): 18 g L^{-1} to encompass the range and to reflect results after a preliminary investigation of the limits in OFAT results (as carbon catabolite repression was observed beyond 30 g L^{-1} soluble starch).

Fermentation factors at their assigned ratio on $Y_{p/x}$ are described in **Table 4.4**. It shows the interaction with factor's average effect at their individual assigned ratio on higher $Y_{p/x}$ by *A. giganteus* MTCC 8408 in submerged fermentation.

Table 4.4 Taguchi DOE L_8 OA with selected factors on $Y_{p/x}$

Run no.	Columns								
	1	2	3	4	5	6	$Y_{p/x}$ (mg gdcw^{-1} L^{-1}) ± SD[a]	S/N ratio	Mycelial biomass (gdcw L^{-1} ± SD)[a]
1	1	1	1	1	1	1	0.517 ± 0.0280	−5.769	25.05 ± 0.35
2	1	1	1	2	2	2	0.729 ± 0.0220	−2.758	21.90 ± 0.48
3	1	2	2	1	1	2	0.9045 ± 0.002	−0.872	22.10 ± 0.78
4	1	2	2	2	2	1	0.415 ± 0.0190	−7.667	27.65 ± 0.65
5	2	1	2	1	2	1	0.4015 ± 0.009	−7.934	29.85 ± 0.80
6	2	1	2	2	1	2	0.519 ± 0.0340	−5.753	24.95 ± 0.54
7	2	2	1	1	2	2	0.83 ± 0.01250	−1.621	21.05 ± 0.42
8	2	2	1	2	1	1	0.611 ± 0.0040	−4.280	26.15 ± 0.23

It can be seen from the **Table 4.5** that INTER COLS 2 × 4 (L_2 - L_1 = 3.662) showed stronger influence compared to other factors followed by K^+/Ca^{2+} level (L_2 - L_1 = 1.943) in afp production. **Figure 4.3** represents the influence of average effect of factors on afp production by *A. giganteus* MTCC: 8408 in submerged fermentation.

At individual ratio, the higher $Y_{p/x}$ was observed with INTER COLS 2 × 4 at level 2 (-2.751) followed by INTER COLS 1 × 2 at level 1 (-3.607).

Table 4.5 Average effects (main effects) of selected factors on $Y_{p/x}$

Columns	Factors	Level 1	Level 2	$L_2 - L_1$
1	C/N ratio	−4.267	−4.897	−0.63
2	K^+/Ca^{2+}	−5.553	−3.61	1.943
3	INTER COLS 1 × 2	−3.607	−5.557	−1.951
4	Mg^{2+}/Na^+	−4.049	−5.115	−1.066
5	INTER COLS 1 × 4	−4.169	−4.995	−0.827
6	INTER COLS 2 × 4	−6.413	−2.751	3.662

Increase in C/N ratio ensued a mere reduction in $Y_{p/x}$ up to level 2 (-4.267 to-4.897) while at individual level, increase in Mg^{2+}/Na^+ ratio ensued significant decrease in $Y_{p/x}$ up to level 2 (-4.049 to -5.115).

All other factors under this category showed variable effect on afp production, suggesting the selected factors and their levels were within the ideal average conditions. Presence of mono- and divalent cation had significant effect on cell morphology. The effect of K^+/Ca^{2+} and Mg^{2+}/Na^+ ratio on $Y_{p/x}$ was inversely proportionate.

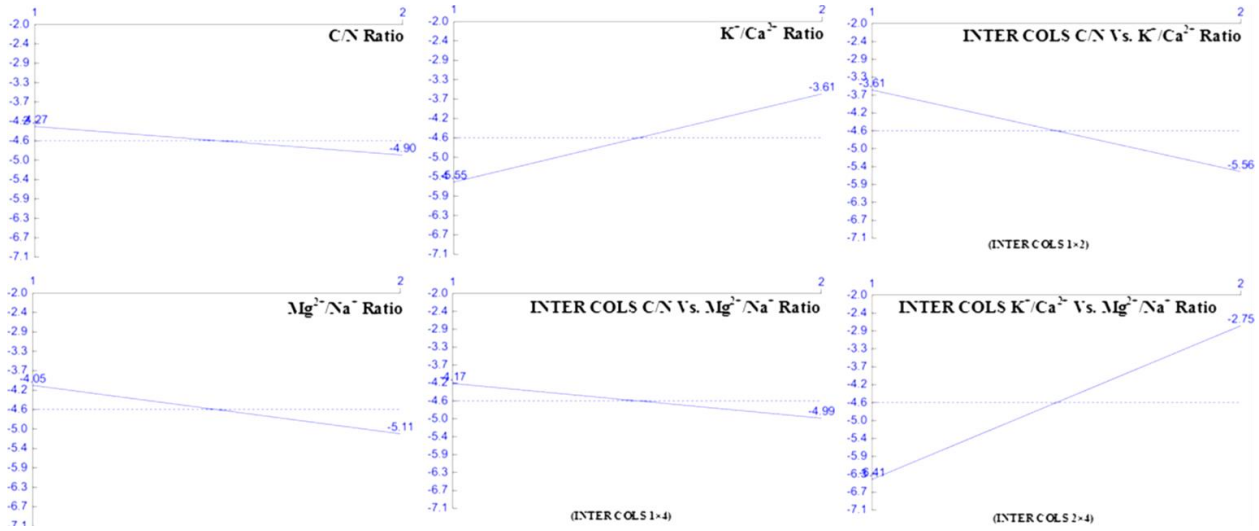

Figure 4.3 Impact of selected factor at their assigned ratio $Y_{p/x}$ by A. giganteus MTCC: 8408 in submerged fermentation

Increase in K^+/Ca^{2+} ratio caused abrupt increase in $Y_{p/x}$ up to level 2 (-5.553 to -3.61) while decrease in INTER COLS 2 × 4 had higher effect on $Y_{p/x}$ at level 2. The impact of factors on higher $Y_{p/x}$ was followed as: INTER COLS 2 × 4 (at level 2) > INTERCOLS 1 × 2 (at level 1) > K^+/Ca^{2+} (at level 2) > Mg^{2+}/Na^+ (at level 1) > INTER COLS 1 × 4 (at level 1) > C/N ratio (at level 1).

4.4.1 Morphological differentiation and biochemical yield

The slowly utilizable soluble starch which favors the metabolite production resulted lower level of μ value but with higher accumulation of intracellular afp in the cell due to the higher $Y_{p/x}$ and μ_{max} value **(Table 4.6).**

Table 4.6 Influence of C/N, K^+/Ca^{2+} and ratio Mg^{2+}/Na^+ on biochemical parameters of various yield in submerged fermentation of *Aspergillus giganteus* MTCC 8408 using Taguchi DOE L_8 OA.

Parameters	Run 1	Run 3	Run 5	Run 7	Run 8
Max. biomass (gdcw L^{-1})	25.05 ± 0.35	22.10 ± 0.78	29.85 ± 0.80	21.05 ± 0.42	26.15 ± 0.23
$Y_{x/s}$ (gdcw g^{-1} L^{-1})	0.835	0.736	0.995	0.69	0.66
μ (D^{-1})	1.63 ± 0.35	1.55 ± 0.31	1.21 ± 0.12	1.11 ± 0.24	1.15 ± 0.23
$Y_{p/x}$ (mg gdcw^{-1} L^{-1})	0.578	0.882	0.385	0.878	0.592
$Y_{p/s}$ (mg g^{-1} L^{-1})	0.483	0.65	0.383	0.616	0.516

Run-3 produced the highest $Y_{p/x}$ and $Y_{p/s}$ than Run-5 in our study. This indicated that soluble starch (45-55% carbon) with low C/N ratio (27.4:1) was propitious to the release of catabolite repression. Run-7 with high C/N ratio (54.9:1) resulted in second highest $Y_{p/x}$ value with least μ value, indicating the effect of catabolite repression was decreased the afp biosynthesis. The influence of various C/N ratio including microelements on afp production was directly controlled and regulated by fungal morphological differentiation **(Figure 4.4).**

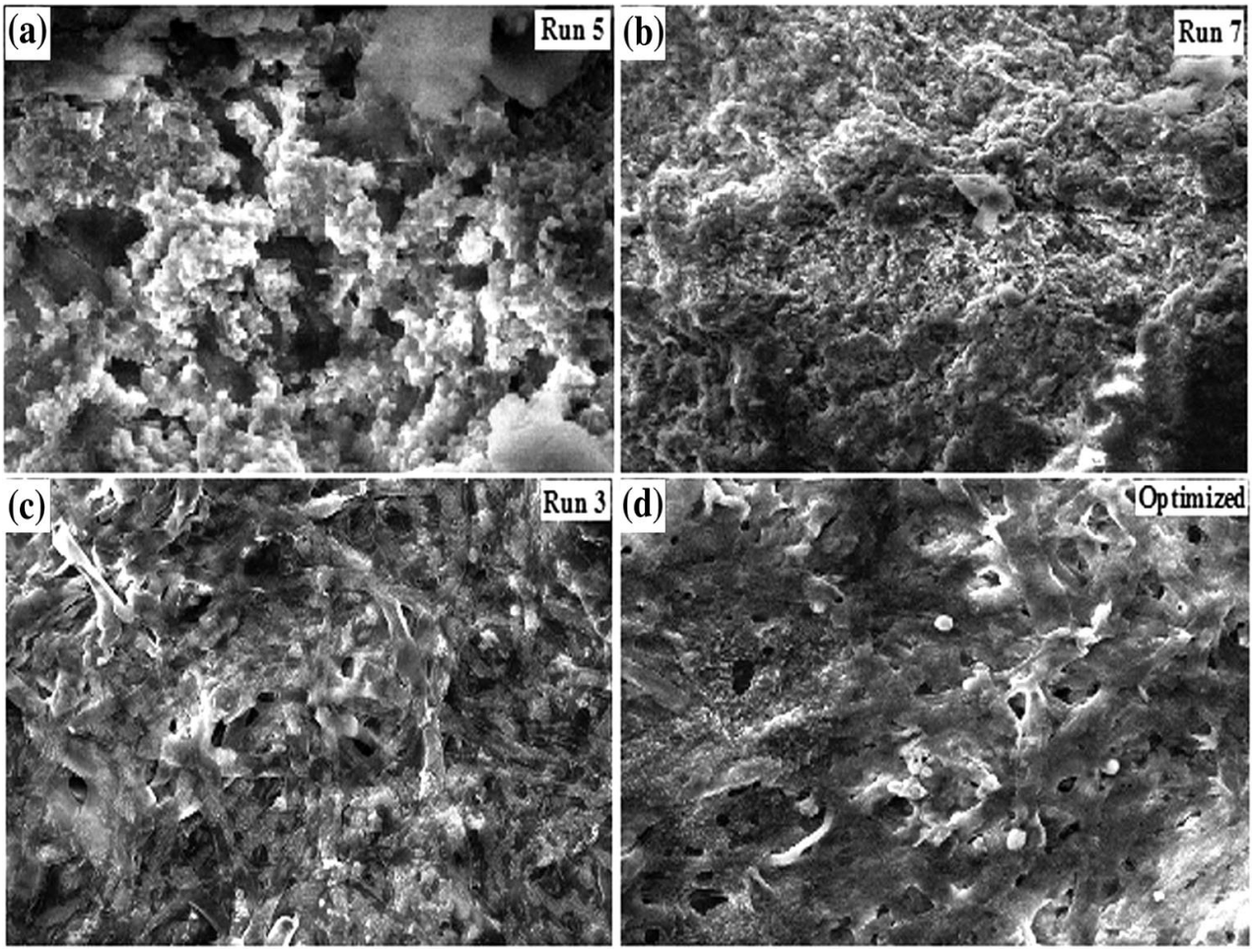

Figure 4.4 Morphological differentiation of *Aspergillus giganteus* MTCC 8408 cell on nutrient dynamics and optimization (a-d). Lateral resolution: 2–10 lm; magnification: 5KX; EHT: 18.00 kV; WD: 9.5 mm

In slowly utilizable soluble starch and corn steep liquor (1.5-3% nitrogen) with proteose peptone (11-12% nitrogen) mycelium was developed thriftily to bigger and looser coarse form with thicker hairy outer region. Tardy assimilation of soluble starch not only supports growth but also self maintenance and survival, compact and bulbous, spongy filamentous with too much sporangium on the tips of hyphae. Highest value of μ was obtained at Run-1 (1.63 ± 0.35 D^{-1}) with low C/N ratio (27.4:1) resulted in second highest $Y_{x/s}$ and second lowest $Y_{p/s}$ value.

This indicated that the faster cell growth resulted in undesired fungal morphology which was inconsistent with the requirement of nutrients **(Figure 4.4a).** Therefore, the carbon catabolite repression occurred in the process with high C/N ratio (54.9:1) in the media. The slowly utilizable soluble starch was easier to induce fungal morphological differentiation which was proved to be propitious to the secondary metabolism.

4.4.2 Analysis of variance (ANOVA)

ANOVA study **(Table 4.7)** showed that among all selected factors INTER COLS 2 × 4 contributed maximally (47.96%) on the overall $Y_{p/x}$ followed by Mg^{2+}/Na^{+} ratio (12.945%) and INTER COLS 1 × 4 (10.151%). All the factors and interactions considered in the experimental design were statistically significant with 90% of confident limit. K^{+}/Ca^{2+} and INTER COLS 1 × 2 showed almost equal contribution of 9.037 and 9.136%, respectively. Negligible contribution was observed with C/N ratio (5.183%) at the individual level on overall production of afp under the aforementioned fermentation conditions, even though it has major impact on mass transfer of nutrients during fungal growth. This study revealed that overall 60.905% contribution was noticed with only two selected parameters (INTER COLS 2 × 4 and Mg^{2+}/Na^{+} ratio) and rest 33.507% by other selected factors (negligible error, 5.588%). From ANOVA evaluation, the impact of factors on the overall afp production was observed as: Mg^{2+}/Na^{+} ratio > K^{+}/Ca^{2+} > C/N at their assigned individual ratio under the Taguchi DOE L_8 OA projection.

Table 4.7 Analysis of variance (ANOVA) under Taguchi DOE L_8 OA

Columns	Factors	DOF	Sum of sqrs.	Variance	F-ratio	Pure sum	% contribution
1	C/N ratio	1	0.795	0.795	0.258	2.541	5.183
2	K^+/Ca^{2+}	1	7.553	7.553	2.451	4.471	9.037
3	INTER COLS 1 × 2	1	7.602	7.602	2.467	4.52	9.136
4	Mg^{2+}/Na^+	1	2.27	2.270	0.736	5.346	12.945
5	INTER COLS 1 × 4	1	1.365	1.365	0.443	3.976	10.151
6	INTER COLS 2 × 4	1	26.812	26.812	8.700	23.731	47.960
Other error		1	3.081	3.081			5.588
Total		7	49.481				100

4.4.3 Taguchi's DOE L_8 OA validation

Based on detailed analysis, optimized condition for maximum afp production could be at C/N ratio: 27.4:1; K^+/Ca^{2+} ratio: 4.78:1; Mg^{2+}/Na^+ ratio: 0.62:1; The expected $Y_{p/x}$ at optimum conditions was 1.054 (based on S/N = 0.457) with total contribution from all the factors was 1.78 (based on S/N = 5.035) with grand average performance of 0.59 (based on S/N = -4.582 mg L^{-1}). The observed 68.88% grand average performance of the fungal strain and 44.02% contribution of all fermentation factors revealed the potential of the fermentation factors concentration and their interaction for afp production by the fungus, *A. giganteus* MTCC: 8408. **Figure 4.5** depicts the severity index (SI) and performance distribution of current condition along with improved condition. The overall enhancement of $Y_{p/x}$ was 44.02% i.e. from 0.59 to 1.054 can be achieved. Further to validate the proposed DOE, experiments were performed for afp production by employing the optimized culture conditions. The experimental data showed an enhanced $Y_{p/x}$ yield by 47.32% i.e. from 0.59 (based on S/N = -4.582 mg L^{-1}) to 1.12 with mycelial biomass 23.9 ± 3.9 gdcw L^{-1}, thus proving the validity of the method with the new modified culture conditions.

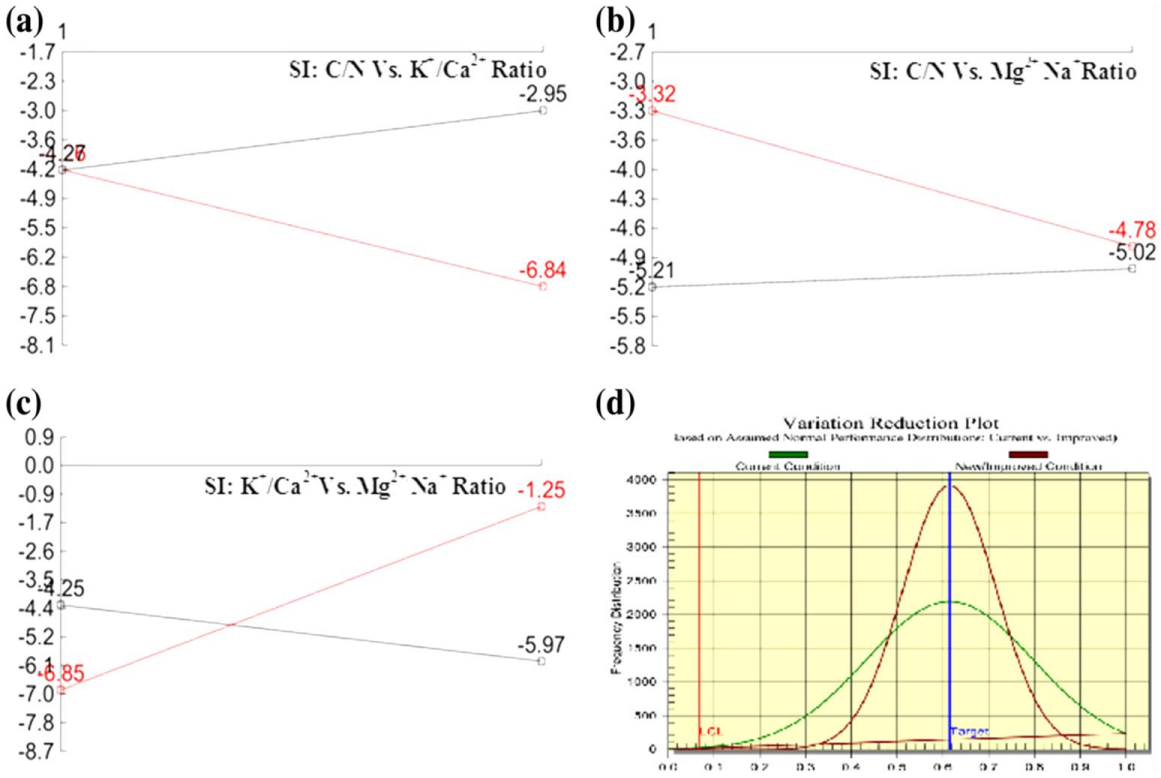

Figure 4.5 Severity index interaction plot and performance distribution plot

4.5 Taguchi's DOE L_{27} OA (final phase submerged fermentation)

Based on Taguchi DOE L_8 OA results, final phase submerged fermentation was performed in broth containing (g L^{-1}): $MgSO_4$, $7H_2O$: 0.4; $CaCl_2$: 0.03; NaCl: 0.3, with eight most decisive factors at their assigned individual level.

4.5.1 Main effect study

The main effects of the fermentation factors at their individually assigned levels on afp production was elucidated using Taguchi's DOE L_{27} OA that explained the average of obtained results (based on S/N value). Certainly, the observed variation indicates the important role of 8 most decisive factors in achieving the best possible combination for optimization **(Table 4.8).**

Table 4.8 Taguchi DOE L27 OA projection with selected factors for afp production in submerged fermentation of *A. giganteus* MTCC 8408

Run No.	Columns								Afp (mg L^{-1} ± SD)	S/N ratio	Cell biomass (gdcw L^{-1} ± SD)
	1	2	3	4	5	6	7	8			
1	1	1	1	1	1	1	1	1	16.6 ± 0.2	24.4	24.6 ± 0.35
2	1	1	1	1	2	2	2	2	14.5 ± 0.2	23.224	23.1 ± 0.48
3	1	1	1	1	3	3	3	3	12.3 ± 0.2	21.794	16.1 ± 0.78
4	1	2	2	2	1	1	1	2	10.05 ± 0.15	20.04	15.3 ± 0.65
5	1	2	2	2	2	2	2	3	10.6 ± 0.2	20.501	15.1 ± 0.8
6	1	2	2	2	3	3	3	1	12.0 ± 0.2	21.58	17.9 ± 0.54
7	1	3	3	3	1	1	1	3	7.85 ± 0.25	17.884	11.2 ± 0.42
8	1	3	3	3	2	2	2	1	8.5 ± 0.3	18.572	10.8 ± 0.23
9	1	3	3	3	3	3	3	2	8.35 ± 0.55	18.377	14.2 ± 0.44
10	2	1	2	3	1	2	3	1	6.05 ± 0.05	15.634	12.7 ± 0.21
11	2	1	2	3	2	3	1	2	5.25 ± 0.35	14.345	10.1 ± 0.88
12	2	1	2	3	3	1	2	3	4.75 ± 0.15	13.52	9.4 ± 0.58
13	2	2	3	1	1	2	3	2	7.0 ± 0.1	16.899	14.2 ± 0.87
14	2	2	3	1	2	3	1	3	6.15 ± 0.25	15.755	12.1 ± 0.41
15	2	2	3	1	3	1	2	1	4.5 ± 0.3	13.006	11.8 ± 0.77
16	2	3	1	2	1	2	3	3	4.85 ± 0.05	13.713	9.9 ± 0.43
17	2	3	1	2	2	3	1	1	4.5 ± 0.4	12.961	8.6 ± 0.9
18	2	3	1	2	3	1	2	2	4.1 ± 0.2	12.224	12.8 ± 0.12
19	3	1	3	2	1	3	2	1	8.4 ± 0.5	18.439	15.8 ± 0.39
20	3	1	3	2	2	1	3	2	7.95 ± 0.15	18.002	14.2 ± 0.29
21	3	1	3	2	3	2	1	3	7.4 ± 0.2	17.375	11.8 ± 0.32
22	3	2	1	3	1	3	2	2	5.4 ± 0.1	14.643	6.7 ± 0.66
23	3	2	1	3	2	1	3	3	5.65 ± 0.45	14.958	9.9 ± 0.21
24	3	2	1	3	3	2	1	1	6.25 ± 0.05	15.916	10.1 ± 0.45
25	3	3	2	1	1	3	2	3	9.85 ± 0.05	19.868	11.9 ± 0.12
26	3	3	2	1	2	1	3	1	10.0 ± 0.2	19.994	14.9 ± 0.38
27	3	3	2	1	3	2	1	2	8.0 ± 0.1	18.059	11.2 ± 0.67

*Mean ± SD (standard deviation) for double determination.

The difference between the average value of each factor at level 2 and level 1 (L_2 - L_1) predict the relative influence of the effect. The larger the difference, the stronger will be the influence. The sign of the difference (1 or 2) indicated whether the change from level 1 to level 2 increased or decreased the result. Stronger influence was observed with pH (L_2 - L_1=1.077 mg L^{-1}) among the factors studied, followed by inoculum level (L_2-L_1=0.651 mg L^{-1}) in afp production (data not shown). Dispersed pulp like morphology was preferred because of higher mass transfer coefficients (low nutrients concentration gradients) with improved afp production compare with pelleted morphology. Change of morphological traits of fungal mycelia at different nutrients composition at their assigned individual level was mentioned in **Fig. 4.6.**

4.5.2 Morphological differentiation

At individual level stage, the higher afp production was observed with soluble starch at level 1 (**Figure 4.6** at Run-1; C/N: 17.88) (20.708 mg L^{-1}) followed by temperature at level 1 (**Figure 4.6** at Run-2; C/N: 17.88) (19.222 mg L^{-1}). Qualitative image analysis showed that *A. giganteus* MTCC 8408 grew as cluster of cell with better spore germination and hyphal growth. Although membrane perturbation due to the induction of intracellular oxidative stress was also noticed. Increase in temperature enhanced reduction of afp production up to level 3 where cell grew as dispersed hyphae with dense branching and retardation of the length of the hyphae as shown in (**Figure 4.6** at Run-7; C/N: 12.51) (17.204 and 15.983 mg L^{-1}). At individual level stage, increase in soluble starch concentration resulted significant decrease of afp production up to level 2 where mycelia grew as swollen and short hyphae with multiple branches (**Figure 4.6** at Run-18; C/N:16.90) (14.229 mg L^{-1}). Higher afp production (17.473 mg L^{-1}) with boisterous distribution, broken hyphal tips and concomitant cell wall immaturation at 10 mm lateral resolutions (**Figure 4.6** at Run-16; C/N:16.90) at agitation up to level 3 (**Figure 4.6** at Run-3; C/N: 17.88) (17.883 mg L^{-1}). All other factors under this category showed variable effect on afp production, suggesting the selected factors and their levels were within the ideal average conditions. Presence of monovalent cation (K^+ at level 1) had significant effect on cell morphology (**Figure 4.6** at Run 15; C/N: 21.03 and Run 6; C/N: 17.88).

Among the 8 most critical fermentation factors studied, the impact of factors on higher afp production was obtained as: soluble starch (at level 1) > temperature (at level 1) > CSL (2%) + proteose peptone (1%) (at level 1) > pH (at level 2) > slant age (at level 1) > agitation (at level 3) > KH_2PO_4 (at level 1) > inoculum vol. (at level 2).

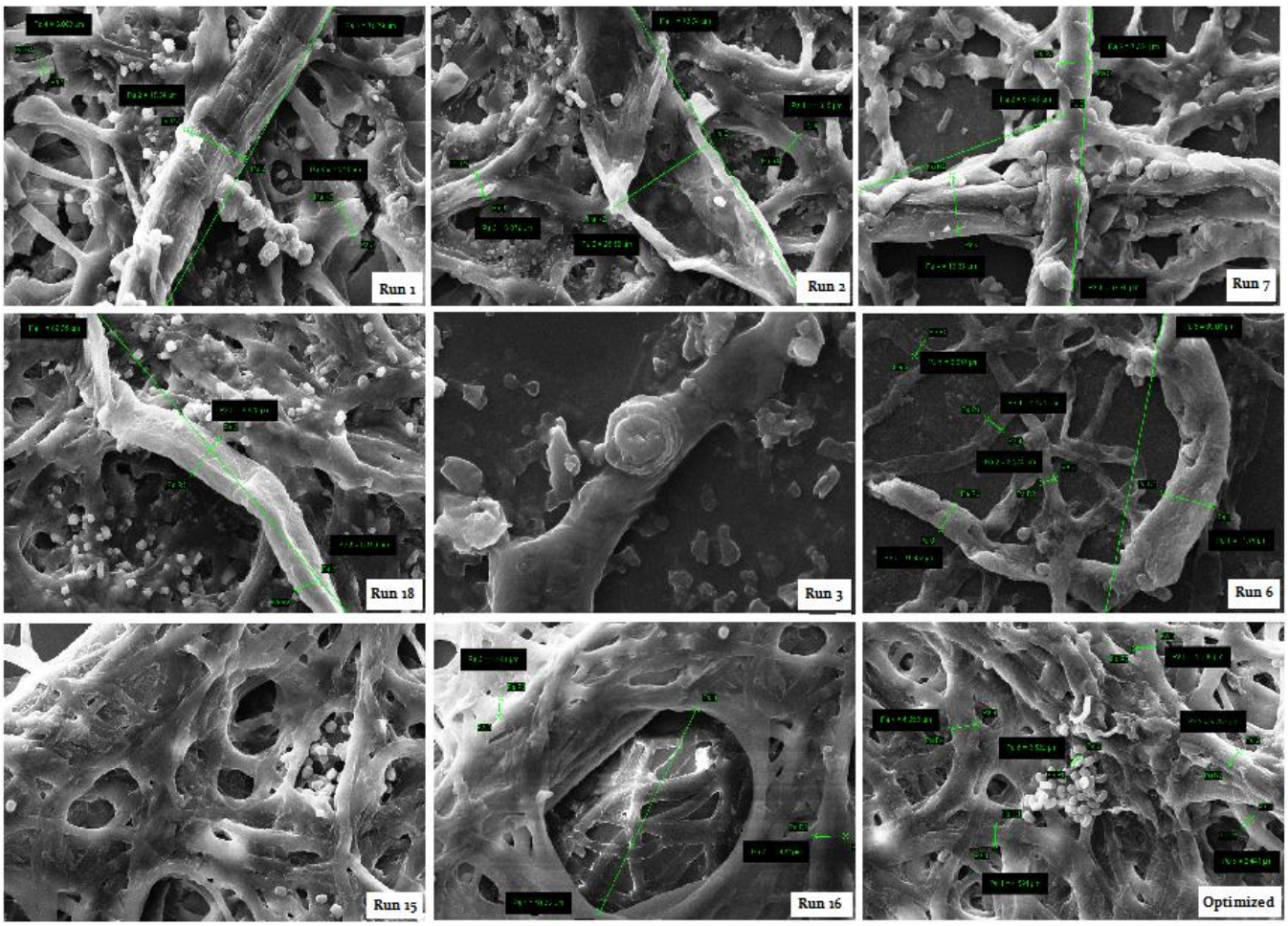

Figure 4.6 Morphological behaviors of *Aspergillus giganteus* MTCC 8408, showing the effect of various nutrients composition on optimization. Lateral resolution: 2–10 mm; magnification: 5KX; EHT: 18.00 KV; WD: 9.5 mm.

4.5.3 Severity index analysis

To have a better perceptiveness on the overall process analysis and the possibility of presence of most interactions, severity index (SI) study was evaluated **(Table 4.9)** from Taguchi DOE L_{27} OA projection that represented the influence of 2 individual factors at various levels of interaction for higher afp production.

Table 4.9 Estimated interaction of severity Index (SI) for selected factors.

Serial No.	Factors	Columns	SI (%)	Reserved column	Level
1	Inoculum vol. × agitation	6 × 7	73.21	1	[1,1]
2	CSL+ PP × pH	2 × 3	69.66	1	[1,1]
3	Inoculum vol. × KH_2PO_4	6 × 8	64.27	14	[2,2]
4	Slant age × agitation	5 × 7	60.68	2	[1,1]
5	pH × Temperature	3 × 4	56.87	7	[1,1]
6	Slant age × KH_2PO_4	5 × 8	55.72	13	[1,1]
7	Slant age × inoculum vol.	5 × 6	53.91	3	[1,1]
8	CSL+ PP × Temperature	2 × 4	52.52	6	[1,1]
9	pH × Agitation	3 × 7	32.19	4	[2,3]
10	CSL+ PP × Inoculum vol.	2 × 6	30.39	4	[1,2]
11	CSL+ PP × KH_2PO_4	2 × 8	20.28	10	[1,1]
12	Soluble starch × pH	1 × 3	19.49	2	[1,1]
13	CSL+ PP × agitation	2 × 7	16.47	5	[1,1]
14	Soluble starch× inoculum vol.	1 × 6	15.95	7	[1,1]
15	Soluble starch × CSL+ PP	1 × 2	15.49	3	[1,1]
16	Temperature × KH_2PO_4	4 × 8	14.78	12	[1,2]
17	CSL+ PP × Slant age	2 × 5	12.91	7	[1,1]
18	Temperature × Agitation	4 × 7	12.15	3	[1,3]
19	pH × KH_2PO_4	3 × 8	10.97	11	[2,1]
20	Soluble starch × KH_2PO_4	1 × 8	10.4	9	[1,1]
21	Soluble starch × agitation	1 × 7	9.08	6	[1,1]
22	pH × Slant age	3 × 5	6.71	6	[2,1]
23	Soluble starch × Slant age	1 × 5	6.69	4	[1,1]
24	agitation × KH_2PO_4	7 × 8	6.31	15	[3,1]
25	Temperature × Slant age	4 × 5	5.48	1	[1,1]
26	pH × Inoculum vol.	3 × 6	4.58	5	[2,3]
27	Temperature× Inoculum vol.	4 × 6	2.28	2	[1,2]
28	soluble starch × temperature	1 × 4	0.87	5	[1,1]

SI analysis indicates relative interactions of factors on the afp production. Interaction SI 100% presents for 90^0 angles between the lines (factors), while 0% SI stands for parallel lines. If the interaction between the factors is reverse, that has been shown by 'Reserved column', 'Levels' indicated the level of factors desirable for the optimum conditions. The highest interaction; SI 73.21% was appeared between inoculum level and agitation (at levels 1 and 1; reserved column 1) among the all interactions followed by SI 69.66% between CSL (2%) with proteose peptone (1%) and pH (at level 1 and 1; reserved column 1). It was interesting to observe that soluble starch (20.708 mg L^{-1} at level 1) and temperature (19.222 mg L^{-1} at level 1) with high impact factor showed least SI 0.87% (at levels 1 and 1; reserved column 5) in combination. On the contrary, the SI interaction between high impact factors slant age (17.947 mg L^{-1} at level 1) and KH_2PO_4 (17.833 mg L^{-1} at level 1) was more than 50% (at levels 1 and 1; reserved column 13).

It was apparent from the observations that the influence of individual factors on afp production had varying effects while in combination; the protein production was entirely independent of the individual influence.

The relative influence of factors and interactions on afp production at chosen levels was mentioned in **Figure 4.7.** Soluble starch has been shown to exert maximum positive impact on the production of afp production in individual cases.

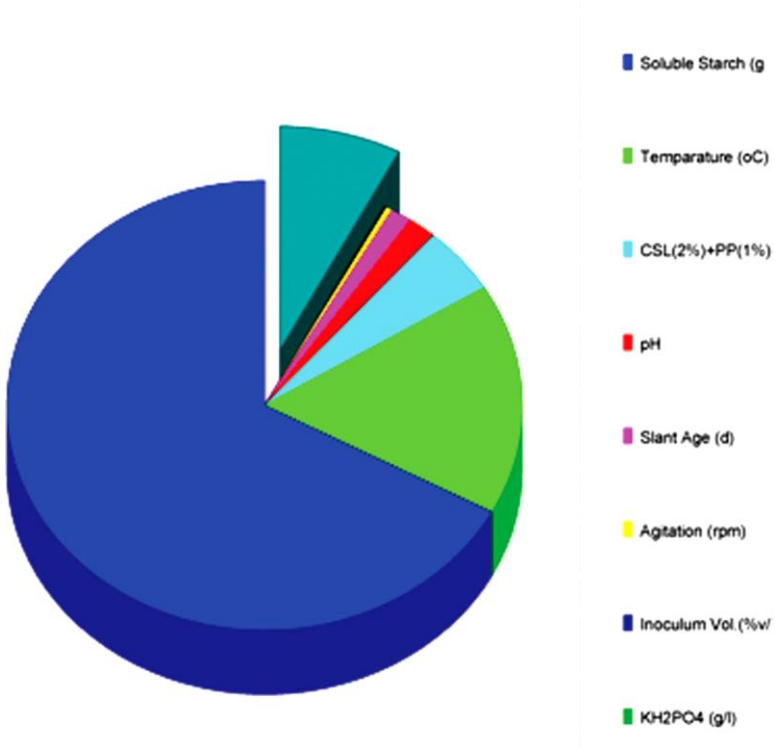

Figure 4.7 Relative influences of factors and interactions.

4.5.4 Analysis of variance (ANOVA)

ANOVA was used to study the data of Taguchi DOE L_{27} OA experiment and to resolve how much variation each factor has contributed **(Table 4.10).** ANOVA Study showed that among all selected factors soluble starch contributed maximally (67.113%) on the overall afp production followed by the incubation temperature (16.672%) and CSL+PP (4.861%).

All factors and interactions considered in Taguchi DOE are statically significant ($p < 0.05$), indicating that the variability of experimental data explained in terms of significant effects. pH and slant age also showed contribution of 1.796 and 1.341%, respectively while KH_2PO_4 showed the least impact (0.054%) at the individual level on overall production of afp under the aforementioned fermentation conditions, even though it has major impact on mass transfer of nutrients during fungal growth. Negligible contribution was observed with agitation and inoculum volume (0.387% and 0.112%).

This study revealed that overall 83.785% contribution was noticed with only 2 selected parameters (soluble starch and incubation temperature) and rest 8.551% (with negligible error, 7.664%) by other 6 selected factors. From ANOVA evaluation, the impact of factors on the overall afp production was observed as: soluble starch > temperature > CSLC proteose peptone > pH > slant age > agitation > inoculum vol. > KH_2PO_4 at their assigned individual level under the Taguchi DOE L_{27} OA projection.

Table 4.10 Analysis of Variance (ANOVA) under the Taguchi DOE L_{27} OA.

Columns	Factors	DOF	Sum of squares	Variance	F-ratio	Pure sum	%contribution
1	Soluble Starch	2	188.918	94.459	114.928	187.274	67.113
2	CSL+PP	2	15.210	7.605	9.253	13.566	4.861
3	pH	2	6.655	3.327	4.048	5.011	1.796
4	Temperature	2	48.167	24.083	29.302	46.523	16.672
5	Slant age	2	5.388	2.694	3.277	3.744	1.341
6	Inoculum vol.	2	1.957	0.978	1.191	0.314	0.112
7	Agitation	2	2.725	1.362	1.658	1.082	0.387
8	KH_2PO_4	2	1.796	0.898	1.092	0.152	0.054
	Other/Error	10	8.218	0.821		7.664	
	Total	26	279.039			100.000%	

4.5.5 Taguchi DOE L_{27} validation

The expected afp production at optimum conditions was 19.42 mg L^{-1} (based on S/N = 25.765 mg L^{-1}) with total contribution from all the factors was 2.64 mg L^{-1} (based on S/N = 8.294 mg L^{-1}) with grand average performance of 7.53 mg L^{-1} (based on S/N = 17.47 mg L^{-1}). The observed 86.4% grand average performance of the fungal strain and 61.22% contribution of all fermentation factors revealed the potential of the fermentation factors concentration and their interaction for afp production by the fungus, *A. giganteus* MTCC 8408. Performance distribution of current condition versus improved condition was mentioned in **Figure 4.8.**

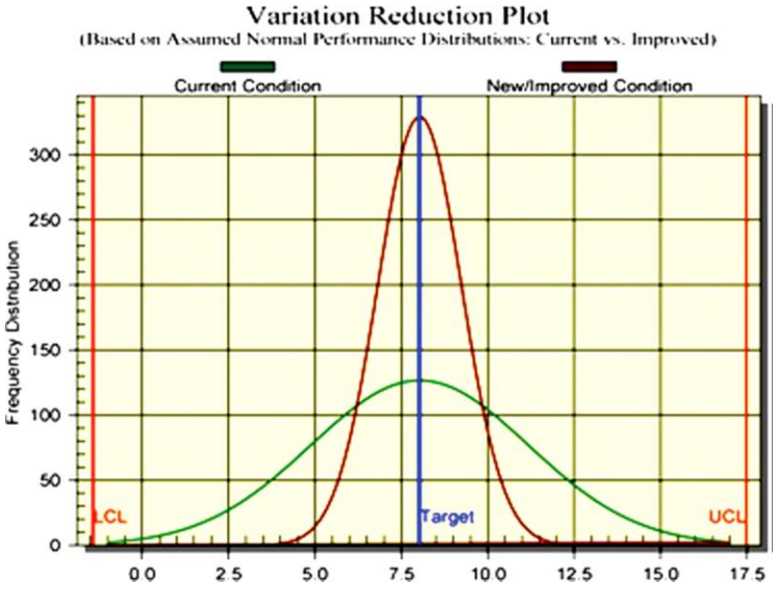

Figure 4.8 Performance distribution plot: current vs. improved condition.

It is evident from the observations that upon considering the optimum culture condition from the Taguchi DOE L_{27} OA, the overall enhancement of afp production of 61.22% i.e. from 7.53 mg L^{-1} to 19.42 mg L^{-1} may be achieved. Further to validate, experiments were performed for afp production by employing the optimized culture conditions **(Table 4.11).**

Table 4.11 Optimum culture conditions and their contribution.

Columns	Factors	Level description	Level	Contribution
1	Soluble Starch	20	1	3.238
2	CSL + PP	30	1	1.056
3	pH	5.8	2	0.701
4	Temperature	25	1	1.752
5	Slant age	3	1	0.476
6	Inoculum vol.	5.0	2	0.296
7	Agitation	180	3	0.413
8	KH_2PO_4	0.1	1	0.363
	Total contribution from all	factors		8.294
	Current grand average	performance		17.470
	Expected result at optimum	condition		25.765

The experimental data showed an enhancement of afp yield by 2.46 fold i.e., from 7.53 mg L^{-1} (based on S/N = 17.47 mg L^{-1}) to 18.54 mg L^{-1} (S/N = 25.362 mg L^{-1}) with mycelial biomass 28.2 ± 0.9 gdcw L^{-1}, therefore; proving the validity of the method with the new modified culture conditions (**Figure 4.6** at optimized; C/N: 17.88).

While OFAT approach resulted afp production enhanced from 5.47±0.21 mg L^{-1} to 12.10±0.11 mg L^{-1} with mycelial biomass enhanced from 21.77±0.31 g L^{-1} to 26.6±0.55 g L^{-1} as compare to basal Olson medium.

4.6 Kinetic study of batch fermentation

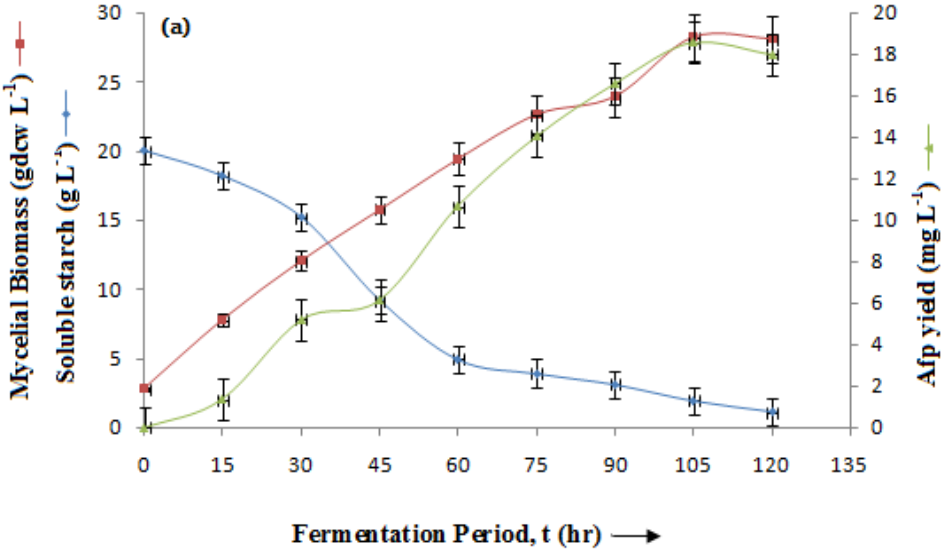

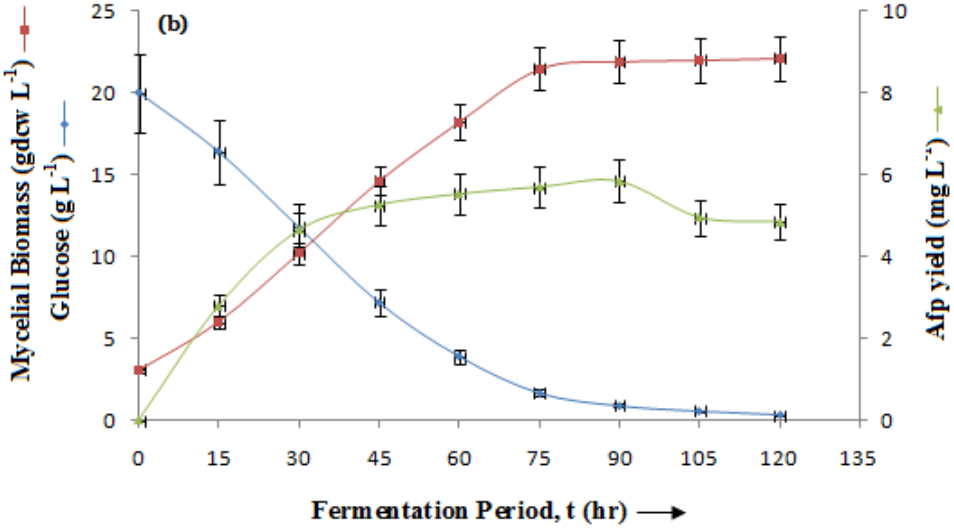

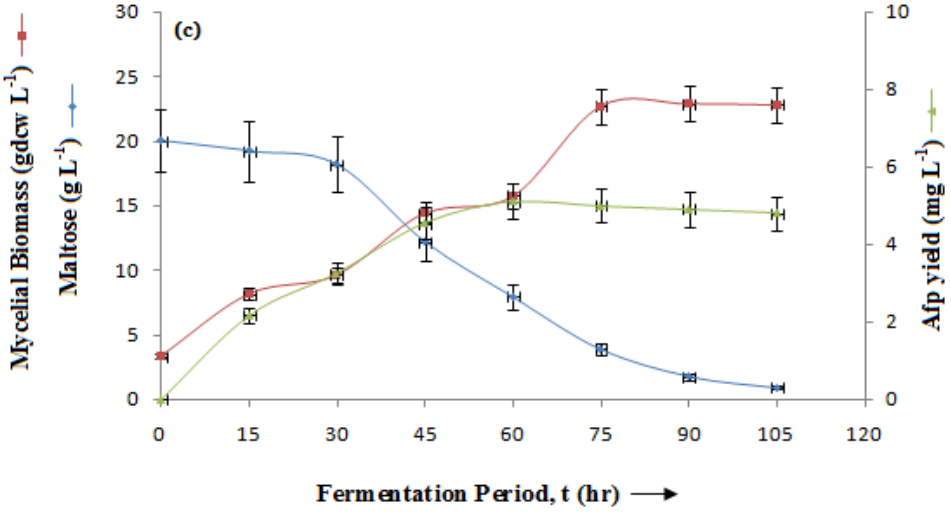
(c)
Mycelial Biomass (gdcw L-1)
Maltose (g L-1)
Afp yield (mg L-1)
Fermentation Period, t (hr)

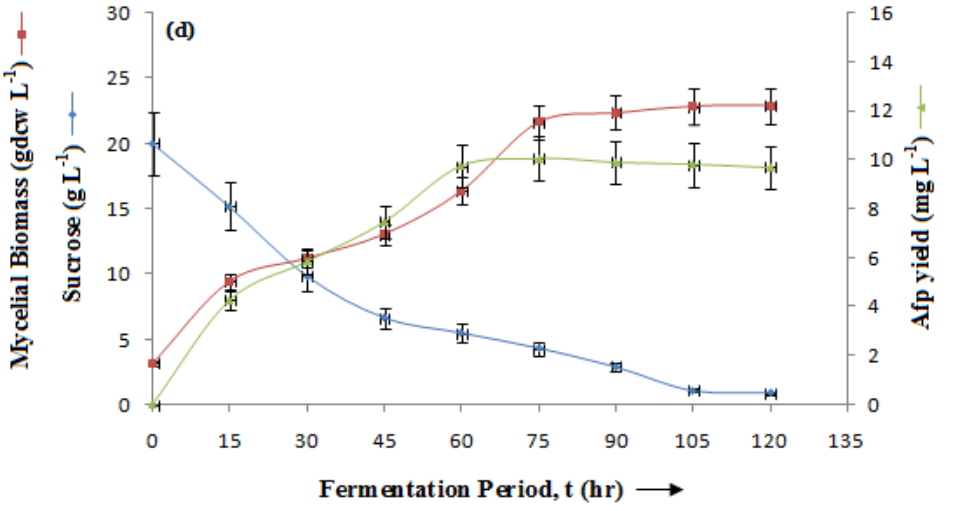
(d)
Mycelial Biomass (gdcw L-1)
Sucrose (g L-1)
Afp yield (mg L-1)
Fermentation Period, t (hr)

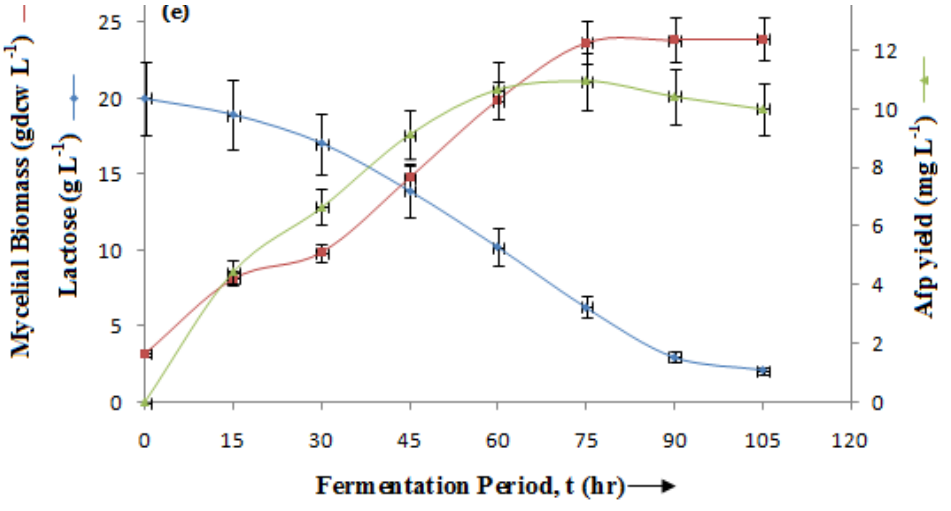
(e)
Mycelial Biomass (gdcw L-1)
Lactose (g L-1)
Afp yield (mg L-1)
Fermentation Period, t (hr)

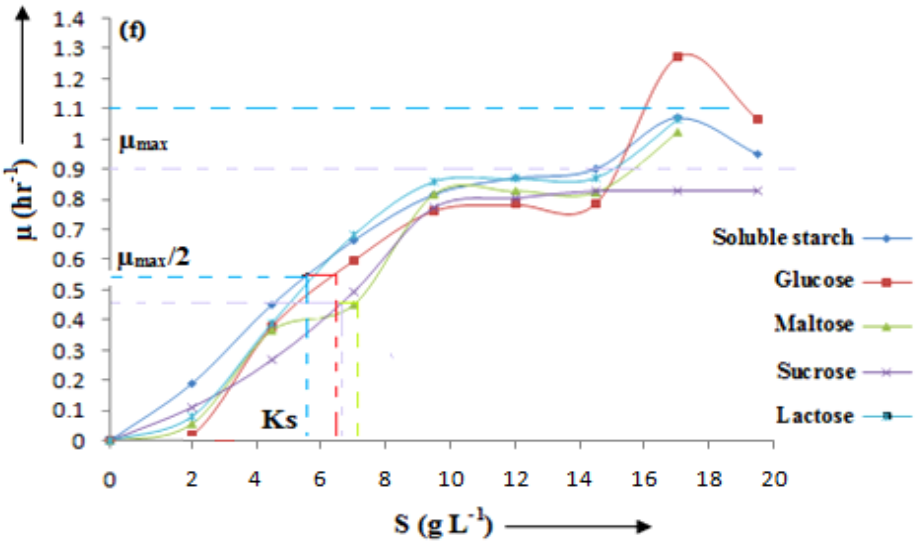

Figure 4.9 A typical time course of carbohydrates consumption, viz., (a) soluble starch, (b) glucose, (c) maltose, (d) sucrose and (e) lactose vs. mycelial biomass and antifungal protein production in submerged fermentation under statistically optimized new modified culture conditions (using Taguchi DOE L_{27} OA), (f) specific growth rate (μ) vs. substrate (S) consumption.

The mycelia level using soluble starch was maximal at the 105 h after inoculation while using glucose, maltose, sucrose and lactose the mycelia level was maximal at the 75 h after inoculation. The maximal productions of antifungal protein by *Aspergillus giganteus* MTCC 8408 utilizing soluble starch in new statistically optimized (Taguchi DOE L_{27}) culture media was at 105 h. when utilizing glucose and maltose The maximal productions of antifungal protein lies in the range 60 h after inoculation and decreased production by about 69% (5.7 mg L^{-1}) and 73% (5.0 mg L^{-1}), respectively. The antifungal protein production was low in maltose (4.8 mg L^{-1}).

Theis et al. **[1, 2, 72]** reported that the maximal concentrations of antifungal protein produced on the 96 h of fermentation in liquid culture medium after inoculation, which are quiet consistent result that obtained in the present study in submerged fermentation. Prolonged cultivation did not further enhance the production of biological active protein compounds already harvested after about 96 h. Consistent with this; we found that more than 82.8% of biologically active compounds were extractable from the mycelia on the 105 h of fermentation. Influence of 8 most influencing factors on biochemical parameters of various yield in submerged fermentation of *Aspergillus giganteus* MTCC 8408 using Taguchi DOE L_{27} OA was evaluated in **Table 4.12.**

Table 4.12 Estimated value of biokinetic parameters in statistically optimized new culture medium using Taguchi DOE L_{27} OA

Parameters	**Soluble starch**	**Glucose**	**maltose**	**Sucrose**	**Lactose**
Max. biomass (gdcw L^{-1})	28.2	22.1	22.9	22.9	23.9
$Y_{x/s}$ (gdcw g^{-1} L^{-1})	1.49	1.121	1.19	1.19	1.7
μ (h^{-1})	0.9	0.788	0.82	0.806	0.86
$Y_{p/x}$ (mg gdcw-1 L^{-1})	0.657	0.264	0.22	0.438	0.458
$Y_{p/s}$ (mg g^{-1} L^{-1})	0.98	0.296	0.267	0.526	0.782

4.6.1 Growth model study

The results of the curve fitting are shown in **Figs. 4.10**. Models such as Monod, Moser, Tessier, Blackman and Haldane failed to fit the experimental data and were omitted. All of the other models tested with the exception of the Logistic model provided reasonably good fitting based on RMSE value (2.45989) observation.

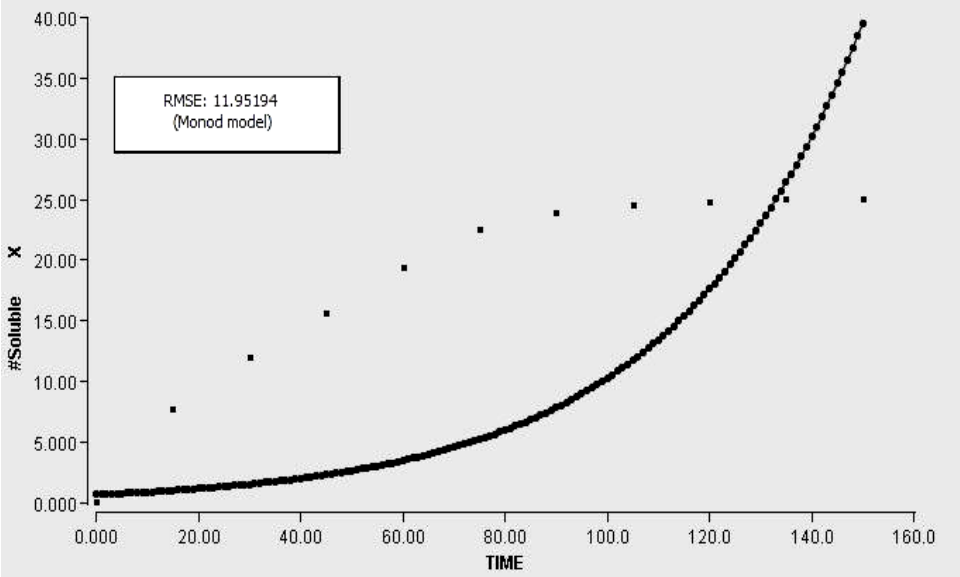

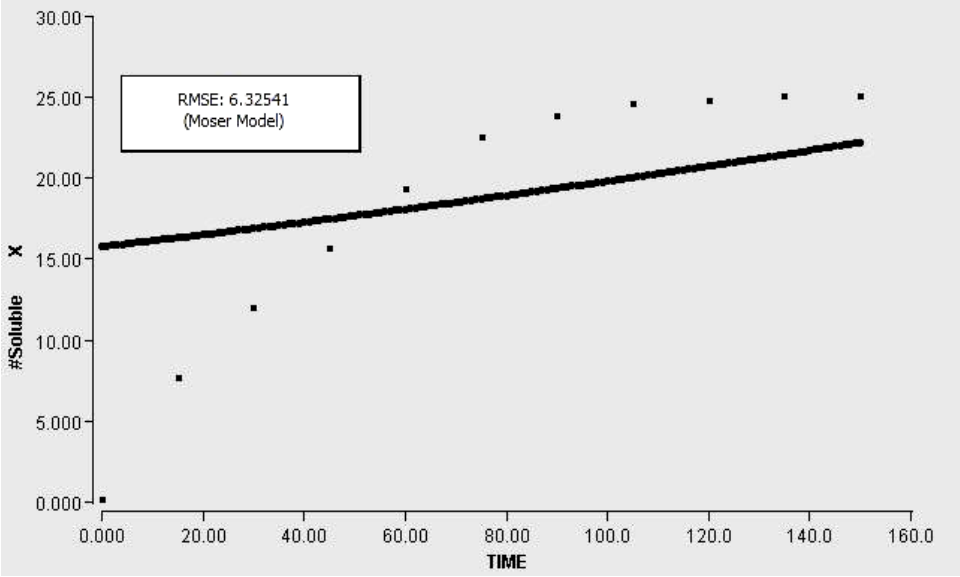

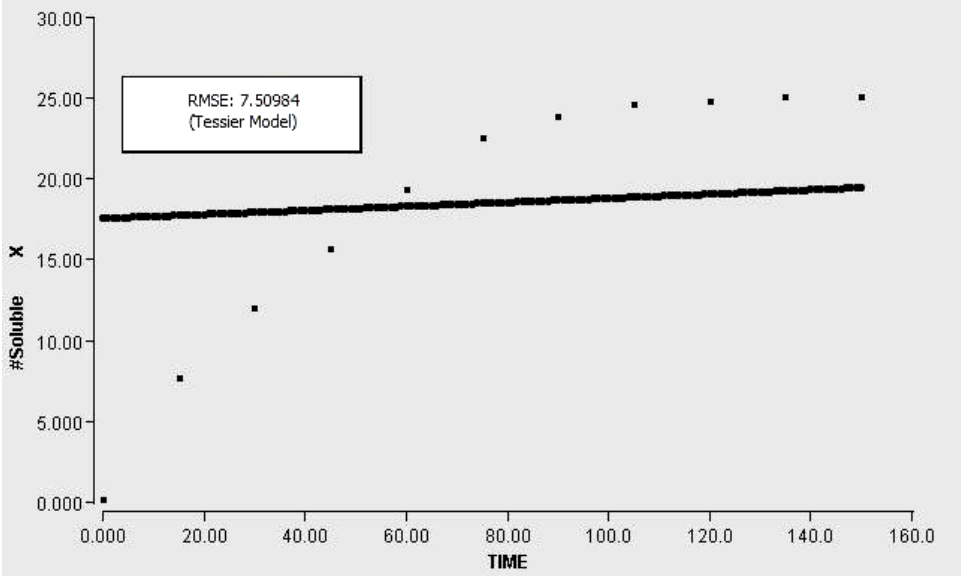
RMSE: 7.50984
(Tessier Model)
#Soluble X
TIME
30.00
25.00
20.00
15.00
10.00
5.000
0.000
0.000
20.00
40.00
60.00
80.00
100.0
120.0
140.0
160.0

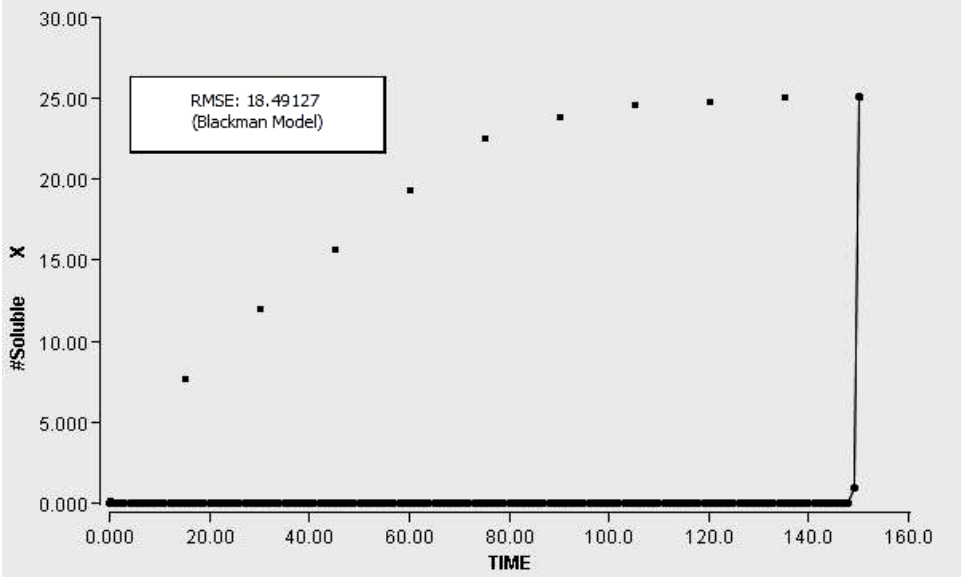
RMSE: 18.49127
(Blackman Model)
#Soluble X
TIME
30.00
25.00
20.00
15.00
10.00
5.000
0.000
0.000
20.00
40.00
60.00
80.00
100.0
120.0
140.0
160.0

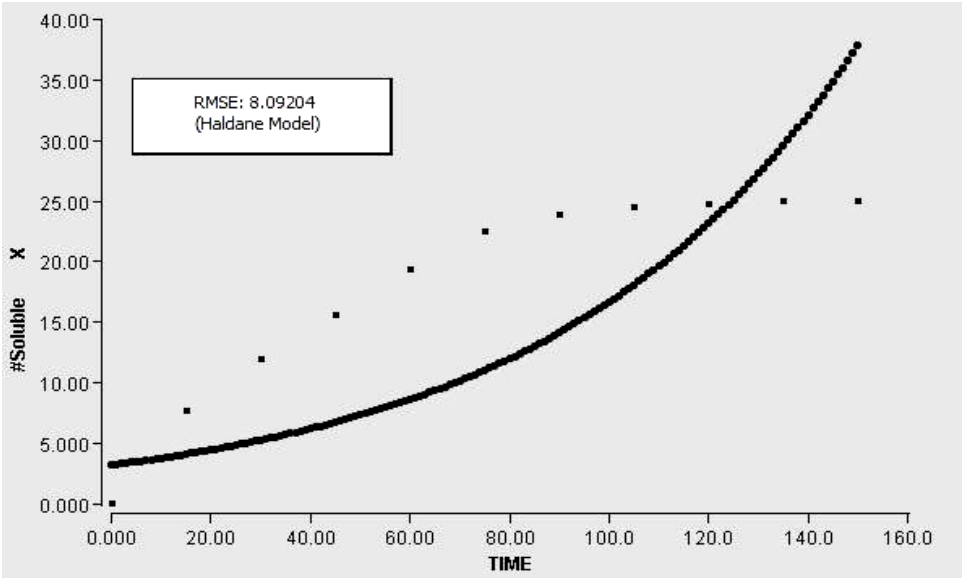

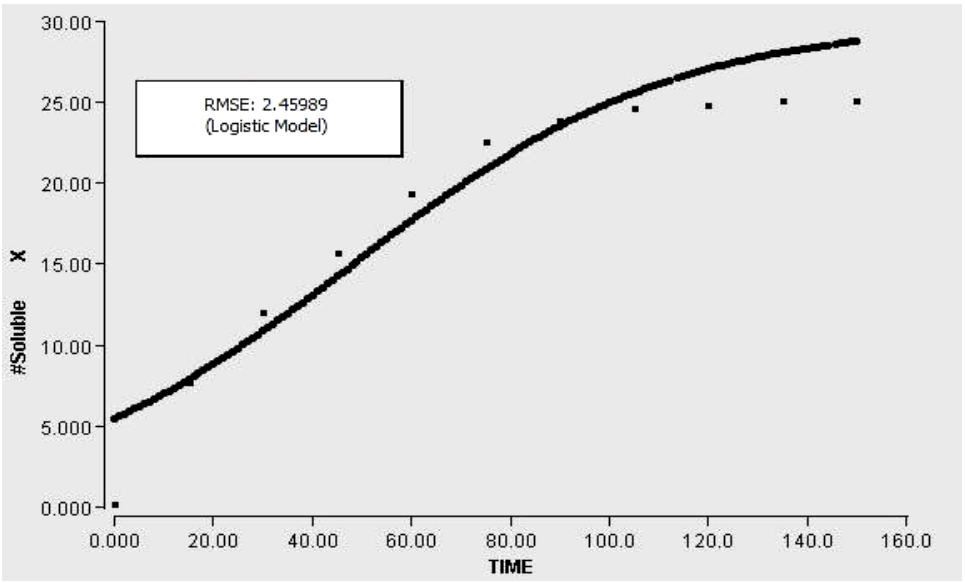

Experimental data; Model predicted data

Figure 4.10 Fitting experimental data and calculated RMSE value with various model, viz., Monod, Moser, Tessier, Blackman, Haldane and Logistic model.

The sigmoidal growth pattern **(Figure 4.10)** of *Aspergillus giganteus* MTCC 8408 in new statistically optimized culture medium (Taguchi DOE L27 OA) was analyzed using a logistic equation for its variation against time to describe the entire fermentation process. Based on the assumptions the following logistic equation was used **[272]** to analyze the growth of *Aspergillus giganteus.*

$$\mu = \mu_{\mathrm{m}}\left(1-\frac{X}{X_m}\right) \qquad \ldots\ldots\ldots\ldots\ldots\ldots\ldots\ldots (4.1)$$

At the beginning of fermentation, when t = 0, the inoculum is considered as the initial concentration, i.e. $X = X_0$. Integrating Eqn (4.1) from t_0 to t gives the explicit form of biomass (X) as a function of time (t):

$$X = \frac{X_{\mathrm{m}}}{1+e^{c-\mu_{\mathrm{m}}\times t}} \qquad \ldots\ldots\ldots\ldots\ldots\ldots\ldots\ldots (4.2)$$

$$\text{Where } c = \ln\left(\frac{X_m}{X_0-1}\right) \qquad \ldots\ldots\ldots\ldots\ldots\ldots\ldots\ldots (4.3)$$

At the abscissa of the inflection point ($t = t_i$) the second derivative of Eqn (4.2) is equal to zero:

$$\frac{d^2X}{dt^2} = 0$$

Therefore;

$$c-\mu_{\mathrm{m}}\times t_i = 0\,;\; t_i = \frac{c}{\mu_{\mathrm{m}}} \qquad \ldots\ldots\ldots\ldots\ldots\ldots\ldots\ldots (4.4)$$

The maximum growth rate ($v_{\max}$) derived by calculating the first derivative of Eqn (4.2), equal to the slope of the tangent to the function at its inflection point (t_i), as

$$v_{max} = \frac{X_m \times \mu_m \times e^{(c-\mu_{\mathrm{m}}\times t_i)}}{\left[1+e^{(c-\mu_{\mathrm{m}}\times t_i)^2}\right]} = \frac{X_m \times \mu_m}{4} \qquad \ldots\ldots\ldots\ldots\ldots\ldots\ldots\ldots (4.5)$$

$$\text{And } (X)_{ti} = \frac{X_m}{1+e^{[(c-\mu_m(c/\mu_m)]}} = \frac{X_m}{2} \qquad \ldots\ldots\ldots\ldots\ldots\ldots\ldots (4.6)$$

The lag period of the culture (λ_x) was defined as the intersection of the tangent at the inflection point with the abscissa axis. The equation of the tangent is, as

$$X_t = X_{ti} + v_{max}(t - ti) \qquad \ldots\ldots\ldots\ldots\ldots\ldots\ldots (4.7)$$

At $X_t = 0$, t becomes λ_x and Eqn (4.7) becomes

$$0 = X_{ti} + v_{max}(\lambda_x - ti) = \frac{X_m}{2} + v_{max}(\lambda_x - ti)$$

$$\lambda_x = \frac{v_{max}(ti) - X_m}{2v_{max}} \qquad \ldots\ldots\ldots\ldots\ldots\ldots\ldots (4.8)$$

$$\text{Substituting } t_i = \frac{c}{\mu_m} \text{ and } v_{max} = \frac{X_m \times \mu_m}{4}$$

$$\lambda_x = \frac{c-2}{\mu_m} \qquad \ldots\ldots\ldots\ldots\ldots (4.9)$$

Substituting c into Eqn (4.2)

$$X = \frac{X_m}{1+e^{[2+\mu_m(\lambda_x - t)]}} \qquad \ldots\ldots\ldots\ldots\ldots\ldots (4.10)$$

Therefore; by linking morphological properties (microscopic variation), Eqn (3.9) to kinetics (macroscopic variation), Eqn (4.1) which allow prediction of specific growth rate, determined in terms of biomass and exponentially growing mycelia during batch culture, provided predicted model for good fitting based on lowest RMSE value observation, as shown…

$$\frac{1}{\mathbf{X}}\frac{d\mathbf{X}}{dt} = \mu_m\left(1 - \frac{\mathbf{X}}{\mathbf{X}_m}\right) + \left(\frac{\mathbf{1.386} \times \mathbf{E}}{\mathbf{G}}\right) \qquad \ldots\ldots\ldots\ldots\ldots (4.11)$$

Table 4.13 Estimated value of morphological parameters in statistically optimized new culture medium using Taguchi DOE L_{27} OA

h_d (µm)	E	N_s	k	N_t	α	L_t (µm)	L_{av} (µm)	G (µm)
15.34	0.81	1.2	0.13	1	1.2	94.54	78.79	94.54
28.02	0.81	1.2	0.13	1	1.2	94.48	78.74	94.48
7.324	0.7	1.2	0.13	1	1.2	81.33	67.78	81.33
9.923	0.93	1.2	0.13	1	1.2	107.71	89.76	107.71
23.33	0.73	1.2	0.13	1	1.2	84.27	70.23	84.27

Figure 4.11 shows predicted model provided reasonably good fitting based on lower RMSE value (0.74204) and lowest AICc value (-76.77) **(Table 4.14).**

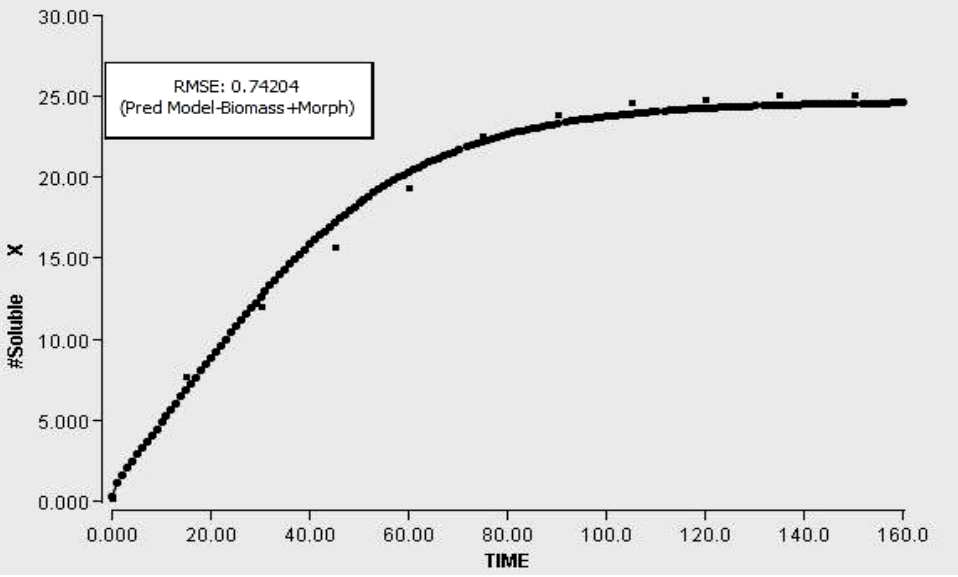

Figure 4.11 Best fitting experimental data and calculated lowest RMSE value in macroscopic model (Logistic) linking with microscopic model (symmetric branching) in exponential growth phase.

Moser and Blackman could fit the data with the best model but the predicted model was with lowest values for RMSE and AICc and highest adjusted R^2 values. The performance of this model is illustrated in simulation profile **(Figures 4.12).** It shows that the dynamics of μ_m, *Ks* and mean extension rate (E) and soluble starch consumption can be well described by the predicted model. The model predicted values for the μ_m, *Ks*, E and S were 0.587 h^{-1}, 0.1 g L^{-1}, 0.066 and 21.25 g L^{-1} respectively, which was consistent with the values reported in the literature **[261].** The length of hyphal growth unit (G) calculated experimentally **(Table 4.13)** was quiet consistent with the published literature (112 µm) **[254].**

Table 4.14 Statistical analysis of predicted kinetic models

Model	P	R^2	SSE	MSE	AICc	AdjR^2	RMSE
Monod	2	0.6346	128.6773	11.6979	36.48	0.5432	11.9519
Haldane	3	0.7406	1641.879	149.2617	60.56	0.6294	8.0920
Tessier	2	0.90413	669.339	60.849	54.62	0.875	7.5098
Moser	3	0.8896	0.0073	0.0006	-65.78	0.8422	6.3254
Blackman	2	0.7832	0.0056	0.0005	-73.87	0.729	18.4912
Logistic	2	0.9	4.9195	0.4472	5.82	0.8801	2.4598
Pred-model	5	0.9953	0.0005	0.00005	-76.77	0.9921	0.74204

Simulation study

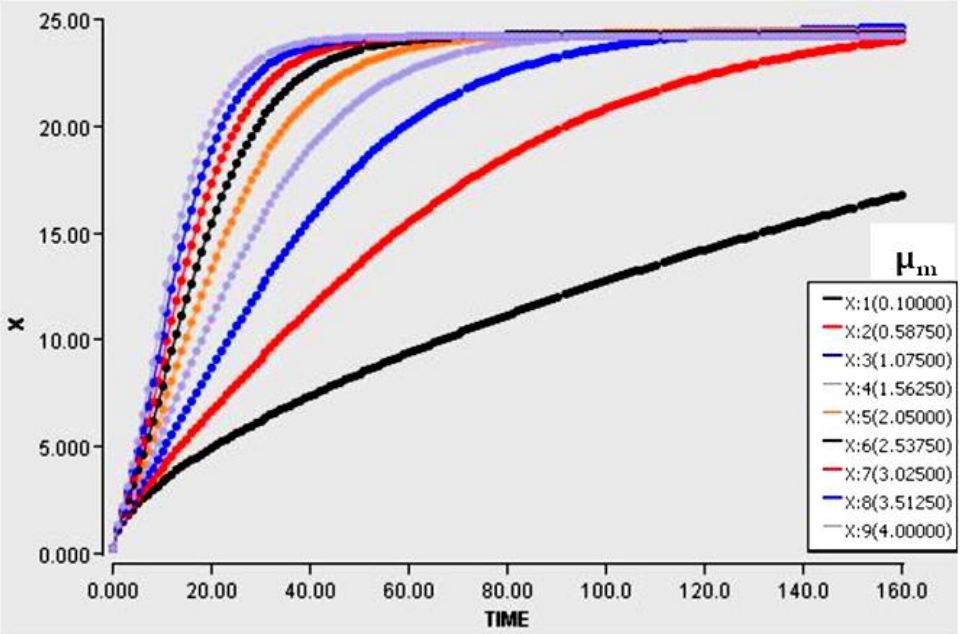

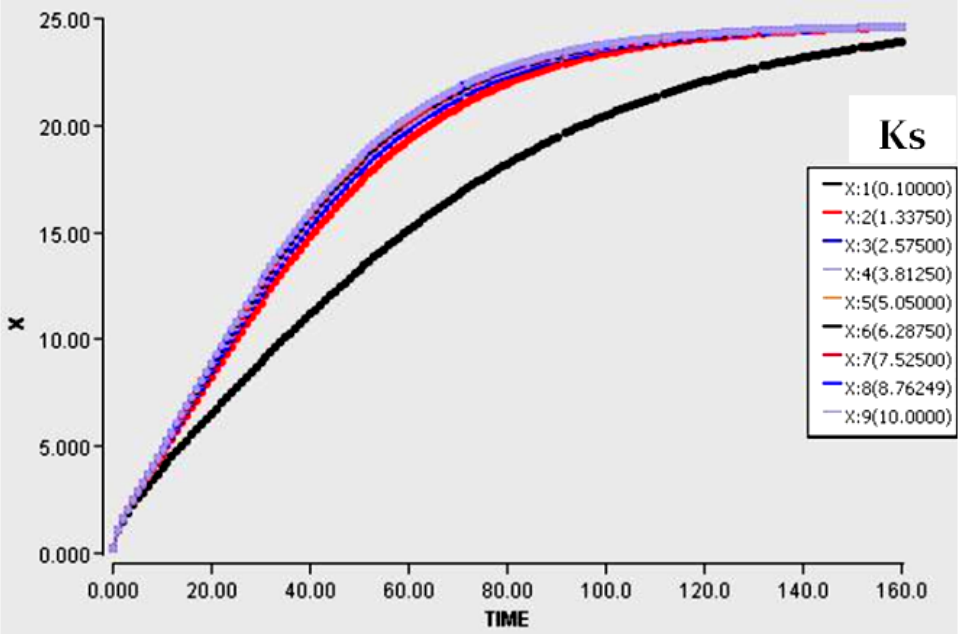

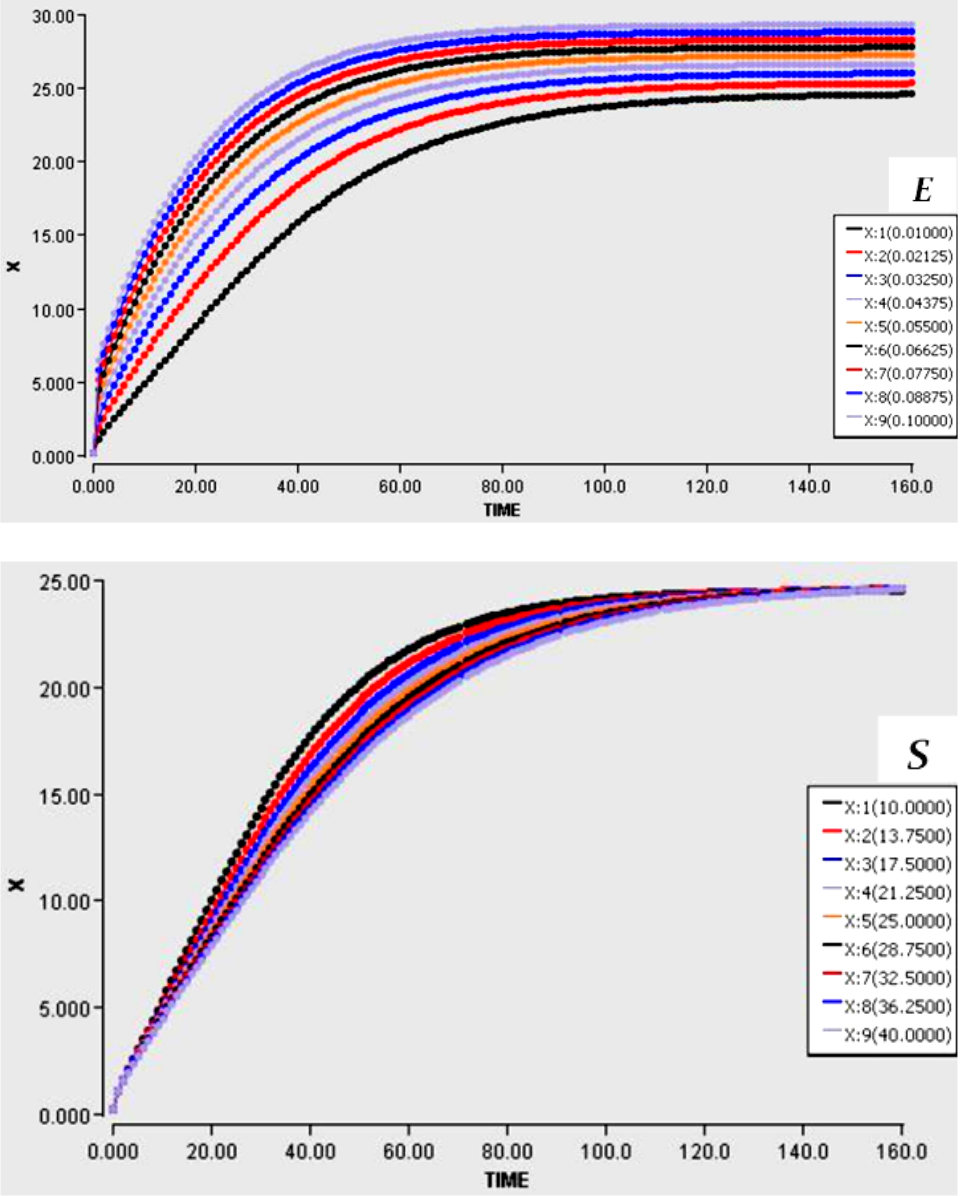

Figure 4.12 Simulation profile of predicted kinetic model with μ_m (max. specific growth rate), K_s (substrate saturation constant), E (mean hyphal extension rate) and S (substrate concentration).

4.7 Isolation and purification of protein

4.7.1 Fractionation-elution profile of the antifungal protein

After sonication and centrifugation under a constant temperature 4^0C, we obtained approximately 108 mL of intracellular solution from approximately 84.6 gdcw of mycelial biomass in total 3 L fermentation broth. To enrich for the active protein, the crude extract was lyophilized (24 hrs at -48^0C, 0.15 mbar) to approximately 36 ml and then fractionated using pure ammonium sulfates (0–30%, 30–50%, 50–70% and 70–90%). Each crude fraction was dialyzed and assayed for growth inhibition against the test pathogens.

Antimicrobial activities were detected (disc diffusion assay) only against *Candida albicans* NCIM 3471 (responsible for invasive candidiasis) in 50-70% $(NH_4)_2SO_4$ fraction. No Antimicrobial activities were detected in other ammonium sulfate fractions viz., 0–30%, 30–50% and 70–90% towards test pathogens (data not shown).

This crude fraction (afp) was passed through a cation-exchange resin carboxymethyl cellulose (CMC) column (2.8 × 20 cm^2) by loading 0.25 ml min^{-1}, and five chromatographic peaks were identified **(Figure 4.13a).**

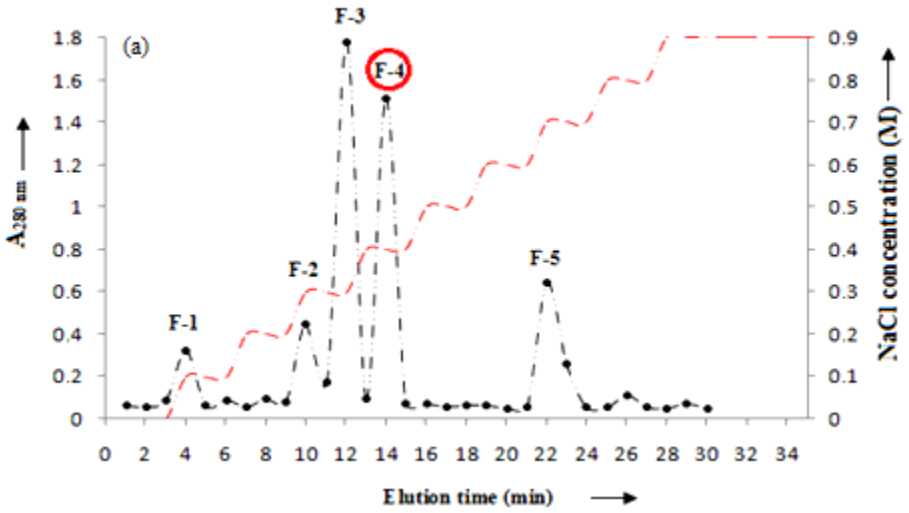

The eluted fractions were assayed for growth inhibition against *Candida albicans*. Chromatography of the fractions resulted in one large unbound peak (F3) and four adsorbed peaks F1, F2, F4 and F5 on the cation exchange column. No antifungal activities were detected in peak F1, F2, F3 and F5 (data not shown); however, antifungal activity was found at 0.4 M NaCl elution in peaks F4 **(Figure 4.13a).**

The fractions corresponding to peaks F4 was then subjected to pass through Sephadex G-100 column (1.6 × 36 cm^2) and eluted with NaCl – 0.05 M sodium acetate buffer (pH 7.4) at the rate of 0.25 ml min^{-1}.

Chromatography of the fractions from peak F4 resulted in a large unbound peak (Pep-1) without any antifungal activity and one small adsorbed peak Pep-2 **(Figure 4.13b).**

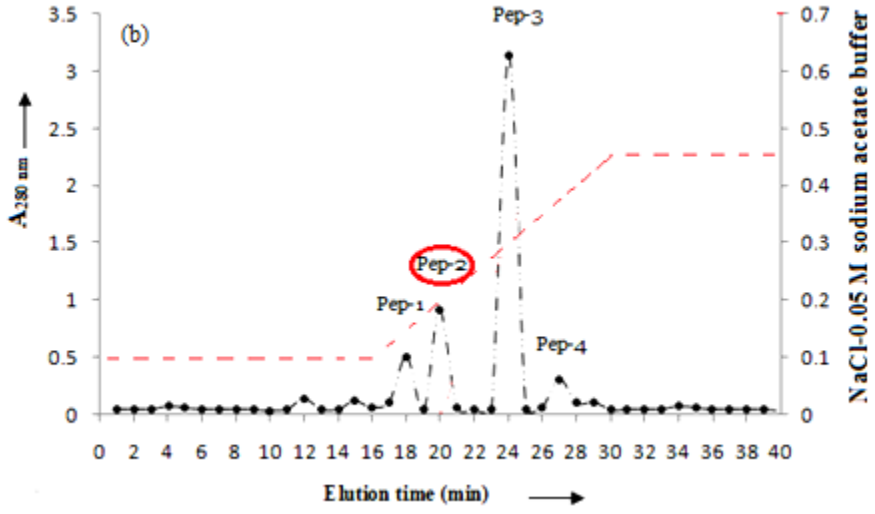

Figure 4.13 Purification of the antifungal protein from the intracellular extract of *Aspergillus giganteus* MTCC 8408, (a) CMC cation exchange chromatography of the crude extract (50-70%), (b) Sephadex-100 gel filtration chromatography of fraction F-4. The eluate was monitored for protein by measurement of the absorption at 280 nm.

The adsorbed peak (Pep-2), eluting between 0.18 and 0.28 M NaCl in 0.05 M sodium acetate buffer (pH 7.4), significantly inhibited the test fungus, *Candida albicans*. After that Pep-2 peak was collected, concentrated and dialyzed, the fraction was analyzed by silver stained SDS–PAGE and a single band was observed on the gel. This antifungal protein was designated as Acp-N84. From 28.2 ± 0.9 gdcw of mycelial biomass, average 4.625 mg of purified Acp-N84 protein (50-70% $(NH_4)_2SO_4$ fraction) was obtained per liter of fermentation broth **(Table 4.15).**

Table 4.15 Purification profile of Acp-N84 from *Aspergillus giganteus* MTCC 8408 in submerged fermentation

Purification step	**Titer value**	**Volume (ml)**	**Total activity**	**Protein concentration (µg/ml)**	**Specific activity**	**Purification ratio (fold)**	**Recovery of activity (%)**
Intracellular supernatant	1024	108	110592	61.74	0.153	1	100
$(NH4)_2SO_4$ fraction (50-70%)	512	30	15360	18.54	0.92	6	62
CMC chromatography	128	15	1920	6.9	1.236	8	56.6
Sephadex chromatography	64	10	640	4.625	1.38	9	17.18

*Total activity calculated as titer × volume; **Specific activity calculated as titer/µg of protein; ***Purification ratio calculated by comparing the value of Specific activity of crude extract vs. purified fraction; ****Recovery of activity calculated by comparing the value of Total activity of crude extract vs. purified fraction

4.8 *In vitro* study

4.8.1 Disc diffusion study

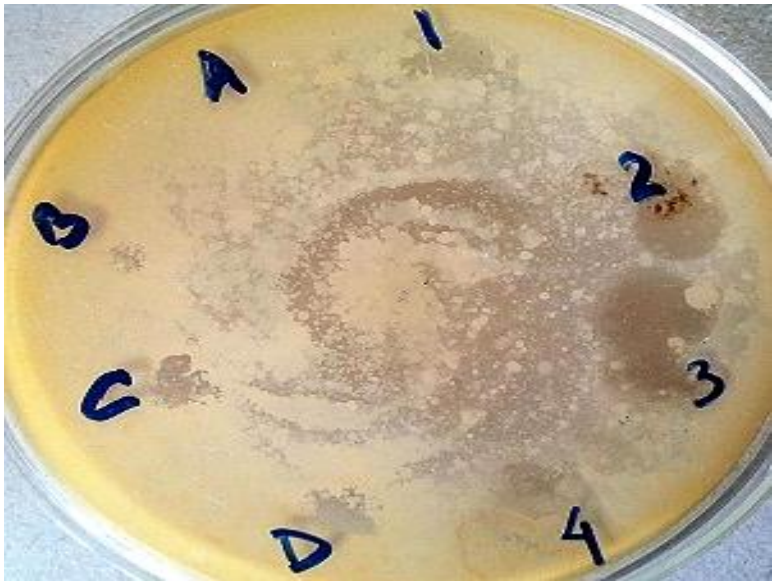

Figure 4.14 Disc diffusion study, crude $(NH_4)_2SO_4$ fraction (100 µl), (A): 70-90%; (B): 30-50%; (C), (D): 50-70% and (1): F4 fraction (100 µl); (2): Pep2 fraction (100 µl); (3): Pep2 fraction (300 µl); (4): Control (buffer).

The antifungal activity of the Acp-N84 against *Candida albicans* exhibited in the concentration range 3.0 (123.46 nM) to 4.0 µg mL^{-1} (164.61 nM). In order to examine the protein concentration required for 90% inhibition of fungal growth (MIC_{90}), dose response plot was studied for five test fungi. The MICs of Acp-N84 for fungal pathogens were in the range of 2.4–3.6 µg mL^{-1}, where *Candida albicans* proved to be the most (MIC: 3.6 µg mL^{-1}) susceptible. MIC values varied between 3.0 and 3.6 µg ml^{-1} for clinically relevant *Candida* species, and these values did not change after prolonged incubation time (at 72 h). *Fusarium oxysporum* and *Aspergillus fumigatus* were not susceptible (<20% inhibition) to Acp-N84 in its investigated concentration range.

In contrast to these results, the applied concentrations of Acp-N84 could inhibit the growth of *A. niger* and *Botrytis cinerea* (<40% inhibition), and considered as ineffective against these isolates in the investigated concentration range.

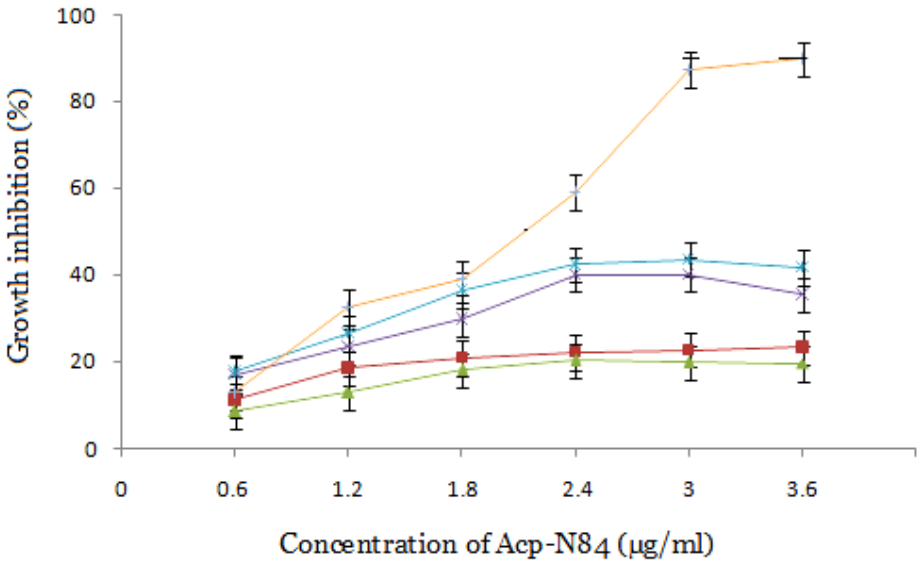

Figure 4.15 Dose response study of Acp-N84. Fungi investigated in *in vitro* antifungal assays were *Candida albicans* ( ), *Aspergillus niger* ( ), *Botrytis cinerea* ( ), *Aspergillus fumigatus* ( ) and *Fusarium oxysporum* ( ). Each data point represents the mean of experiments (n = 3 each) performed two times.

4.8.2 Imaging *in vitro* antibiofilm activity

Biofilm cells typically exhibit increased resistance to antimicrobial agents and the host immune system. *In vitro* antibiofilm activity was studied using various microscopic techniques viz., confocal microscopy, scanning electron microscopy (SEM) and atomic force microscopy (AFM), in order to evaluate ultrastructural changes. For confocal microscopy, the *Candida albicans* biofilm was grown on petri plates using potato dextrose agar (PDA) supplemented with 50 mM of NaCl enables an optimum biofilm growth.

The 48 h biofilm was aseptically transferred into culture plate and rinsed with 0.1M PBS (pH 7.4). For SEM and AFM, after rinsing with 0.1M PBS (pH 7.4), the 48 h biofilm was lyophilized and fixed in 2.5% glutaraldehyde in 0.1 M cacodylate buffer (pH 7.1) onto microscope cover slide. The plate or cover slide was then treated with 100 µl of antifungal protein Acp-N84 (at MIC_{90}) followed by incubation at 37^0C for 24 h and the viability of the biofilm cells was assessed. The ultrastructural changes was imaged with gold coating (for SEM) and with dehydrated in graded alcohol (for AFM).

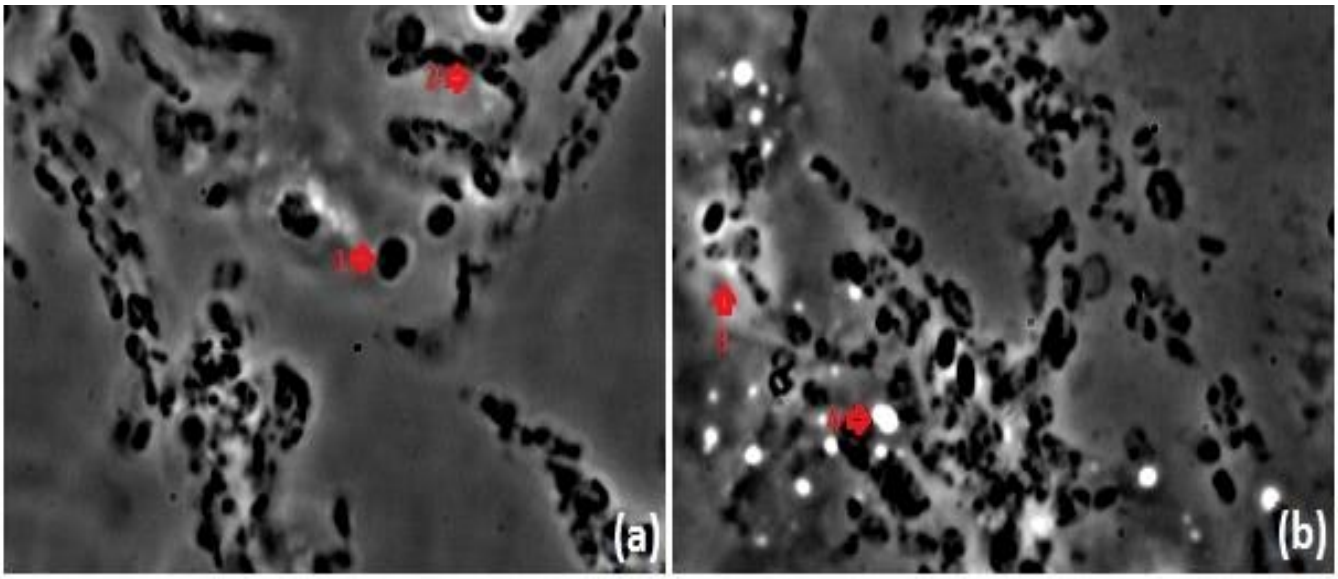

Figure 4.16 Appearance of different cell morphologies of *C. albicans* after treated with 100 µl protein Acp-N84. **(a1)** Aberrant growth forms which occasionally appear in the cultures incubated under conditions that induce germination **(a2)** Germinated blastoconidium bearing mature hyphae, with microspheres massively attached along the whole length of the hyphae, **(b3)** lysis and degradation of intracellular content. **(b4)** abolished attachment of microspheres to blastoconidia bearing short germ tube and dramatically reduced the mycelial populations.

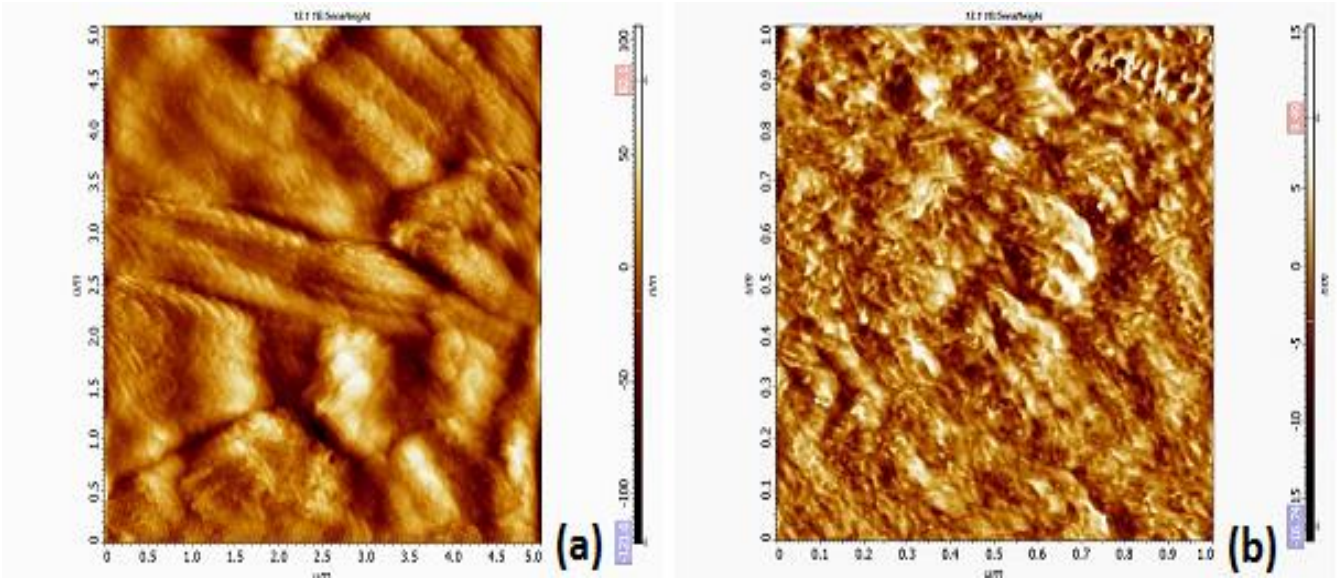

Figure 4.17 Atomic force micrographs showing variation in the height of untreated and treated 100 µl Acp-N84 protein(24 h) *C. albicans* cells: (a) Untreated (h 82.1 nm), (b) treated (h 9.49 nm).

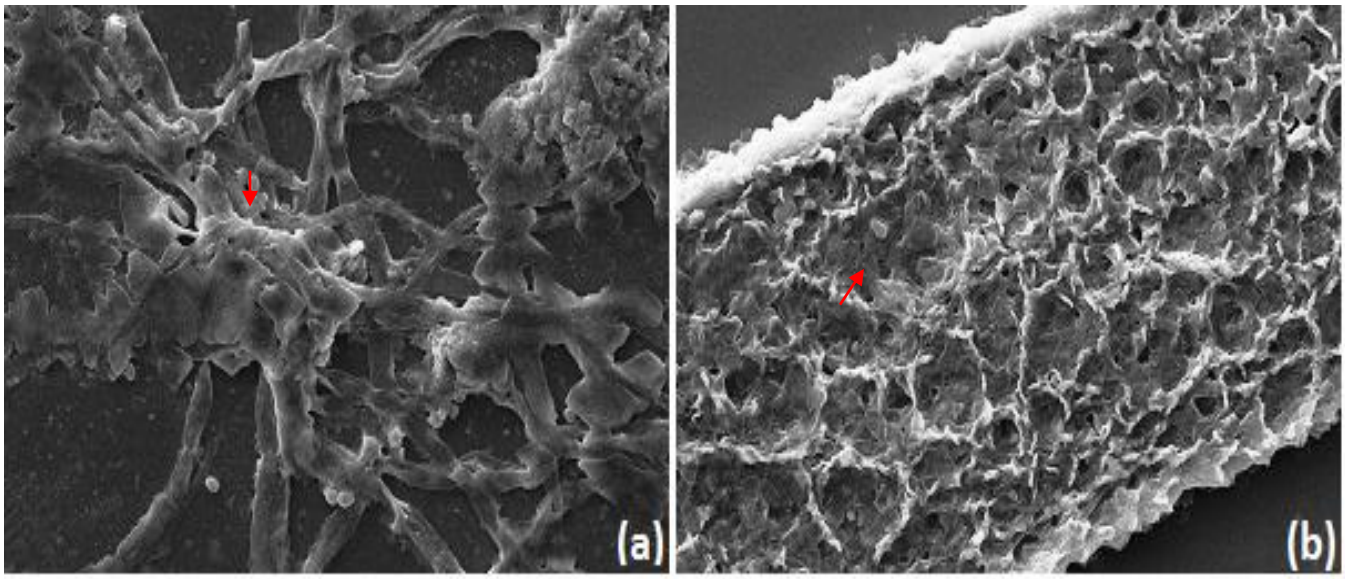

Figure 4.18 Scanning electron micrograph of the 48 h biofilm formed in *C. albicans* **(a)** biofilm formed without antifungal protein Acp-N84, smooth cell membrane of normal cell **(b)** biofilm formed in the presence of 100 µl Acp-N84 protein at MIC_{90}, cell membrane shrinkage in sessile cells, bursting of cells leading to vesicle formation followed by cell wall lysis.

4.8.3 Time killing assay

Anticandidal activity of the intracellular proteins was further studied by considering their time killing profile on *C. albicans* strain (as per standard protocol: CLSI document M27-A2). To compare the efficacy of Acp-N84 with the different types of conventional antifungal agents, the susceptibility of *C. albicans* isolates were also tested to caspofungin (MIC_{90}: 16 µg ml^{-1}), amphotericin B (MIC_{90}: 8 µg ml^{-1}) and fluconazole (MIC_{90}: 64 µg ml^{-1}) as standard antifungal. Time killing profile showed that antifungal protein caused a mean maximum decrease of A_{490} 0.56 to 0.35 (> 90% killing) within 6 h of investigation while amphotericin B and fluconazole decreased the number of viable yeast cell with mean maximum of A_{490} 0.54 to 0.24 and 0.51 to 0.19 respectively (> 99% killing) within 6 h. Fluconazole demonstrated the better killing profile by eradicating the fungal cells rapidly within first 2 h with 0.6 to 0.50 A_{490} reduction (> 90% killing) while amphotericin B displayed a slight reduction in yeast growth showing fungistatic activity against the tested strain.

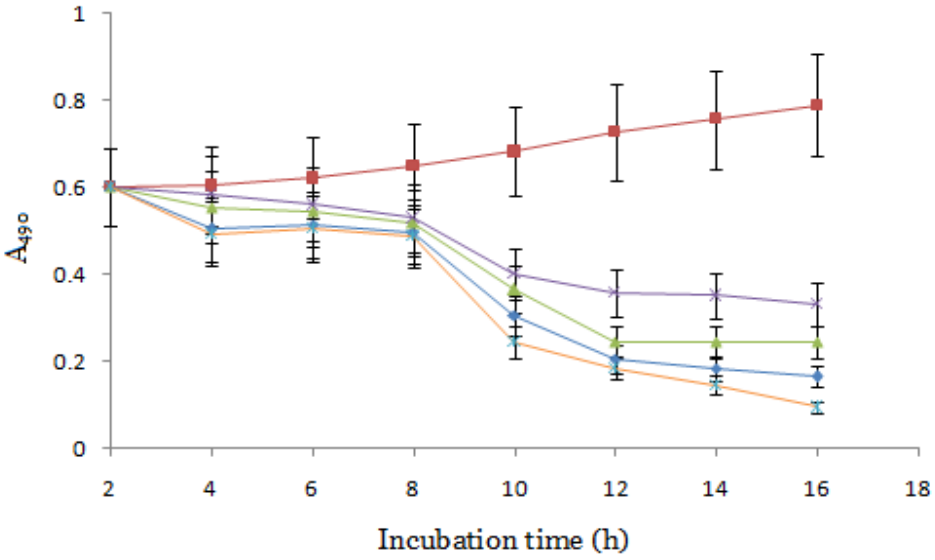

Figure 4.19 Time killing assay of *Candida albicans*, efficacy of Acp-N84 was investigated in *in vitro* with conventional antifungal agents; fluconazole ( ), caspofungin ( ),

amphotericin B ( ), Acp-N84 ( ) and control ( ). Each data point represents the mean of experiments (n = 3 each) performed two times.

4.8.4 Cytotoxicity assay

The cytotoxicity profile of the fungal peptides 1-4 were determined using the MTT assay against HeLa cell line, after 24h treatment with different concentrations of the peptides. The results showed a dose dependent cytotoxicity, where peptide 2 and 4 found to be most active with inhibitory concentration (IC_{50}) value of 5µM for both. But the other two peptides 1 and 3 are less effective with IC_{50} value of > 20µM in case of peptide 1 and about 20 µM in case of peptide 3 **(Figure 4.20).** Thus, we can conclude that out of the four peptides, peptide 2 and 4 are the most effective with antitumor activity and peptide 3 is moderately active whereas peptide 1 is the least effective one against HeLa cells. On the basis of cytotoxicity assay we have further selected peptides 2 and 4 for the study of apoptosis inducing activity.

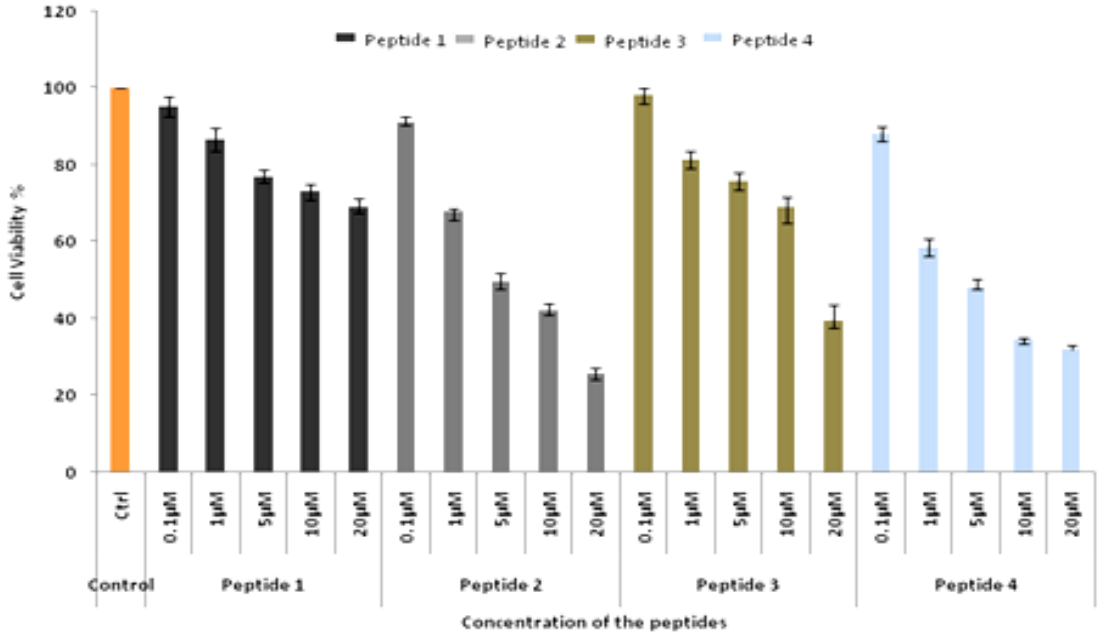

Figure 4.20 Cytotoxicity assay in human cervical cancer (HeLa) cells on treatment with peptides 1-4. HeLa cells were treated with various concentrations of the peptides for 24 h and cytotoxicity was evaluated by MTT assay. Results are expressed as percentage of the control ± SEM of three replicates.

4.8.4.1 Detection of Apoptosis by Hoechst 33342 and Propidium iodide

The nuclear morphological changes in HeLa cells, determined by fluorescence staining with Hoechst 33342 and propidium iodide dye after treatment with peptide 2 and 4 for 24 h has been illustrated in **Figure 4.21**. The live cells appeared to have intact nuclei stained with blue fluorescence. In case of cells treated with the peptides, presence of early and late apoptotic cells was observed. In early apoptotic cells, chromatin condensation and fragmentation with bright blue fluorescence was observed, whereas, in case of late apoptotic cells condensed and fragmented nuclei with pink fluorescence was present. We can also deduce that both the peptides

showed dose dependent apoptotic cell death. Thus, this demonstrates the apoptosis inducing activity of peptides 2 and 4.

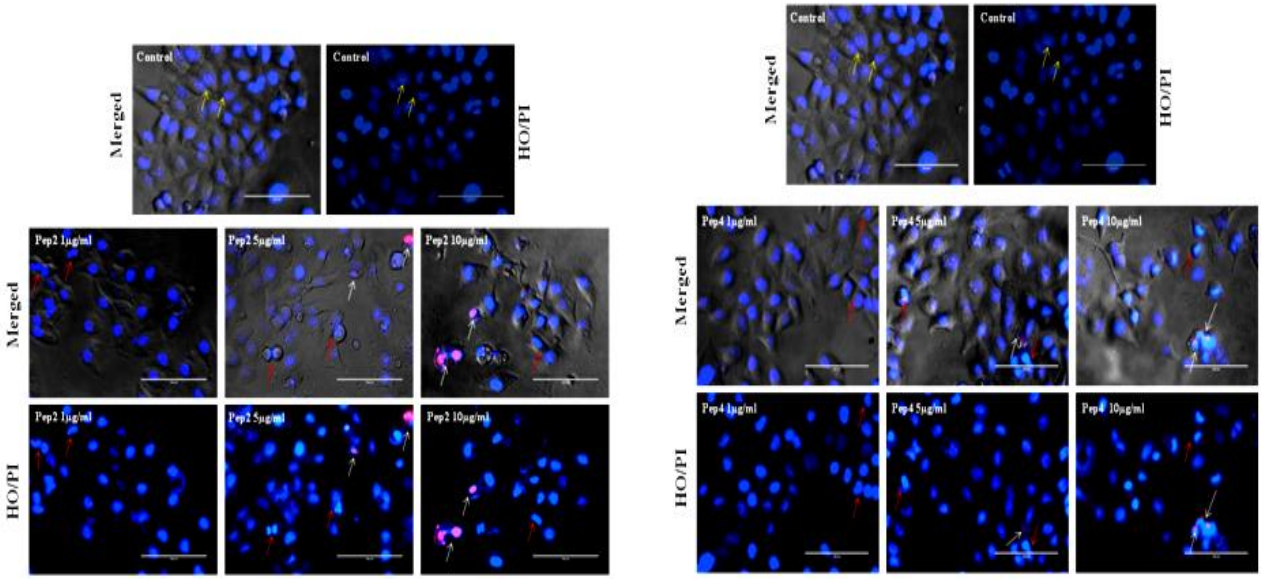

Figure 4.21 Apoptotic detection by Hoechst 33342/Propidium iodide staining in HeLa cells. Nuclear morphological changes on treatment with 1, 5 and 10µM concentrations of peptides 2 and 4 for 24 h in HeLa cells were observed under an inverted fluorescence microscope (EVOS FL). [Yellow arrow shows live cells where as red arrow represents the early apoptotic cells with bright blue condensed or fragmented chromatin), white arrows show late apoptotic cells with pink condensed or fragmented chromatin].

4.9 Molecular characterization

4.9.1 SDS-PAGE

The purified Acp-N84 had an apparent molecular weight of 24.3 kDa as determined by comparison to the molecular weight makers on the silver stained SDS–PAGE and ESI-MS **(Figure 4.22)**. To determine the precise molecular weight of Acp-N84 that was represented by the single band shown in **(Figure 4.22b)**, we evaluated the protein by ESI-MS. The results of the ESI-MS analysis revealed that the molecular mass of the protein was 24645.35 Da **(Figure 4.22a)**, which showed good correlation with its appearance on the protein gel. The average yield of purified Acp-N84 was 4.625 ± 0.87 µg ml^{-1} of fermentation broth (n = 3).

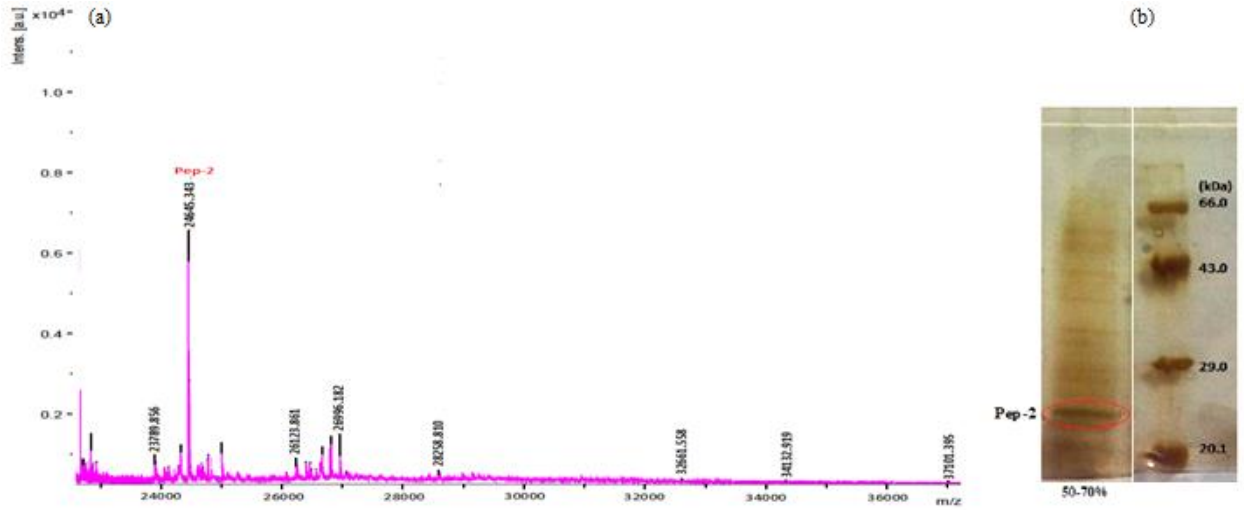

Figure 4.22 SDS–polyacrylamide gel electrophoresis, molecular mass and ESI-MS spectrum of purified Acp-N84 protein. (a) The molecular mass of the purified Acp-N84 was determined using ESI-MS study. (b) Acp-N84 purified by CMC cation exchange chromatography and gel filtration was subjected to SDS–polyacrylamide gel electrophoresis.

4.9.2 FTIR study

Fourier transform infrared (FTIR) spectroscopy is an established tool for the structural characterization of proteins. FTIR data was analyzed using EssentialFTIR 2.0 (Madison, USA) with ATR correction **(Figure 4.23).** Out Of all the amide bands, the most intense and useful band for the analysis of the secondary structure of proteins was amide I band, which represents primarily the CHO stretching vibration of the amide groups (though coupled to in-plane bending of the N–H and stretching of the C–N bonds) and occurs in the region 1600–1700 cm^{-1} as observed. The most useful IR band for the direct measurement of secondary structure of protein is a broad band found between 1660 and 1639 cm^{-1}.

Two sharp bands were observed at 1654.9241 cm^{-1}, characteristic of proteins with predominantly α-helical secondary structures exhibited by amide I band (1650–1658 cm^{-1} and 1635.6360 cm^{-1} (1625–1640 cm^{-1}) may be considered as evidence of the presence of a significant amount of β-sheet secondary structures. The absorption suggestive of β-sheet secondary structures in fact most likely arises from turns within the protein. Two bands at 1624.0631 and 1674.2123 cm^{-1} affirms the presence of an antiparallel β-sheet structure. Presence of ester-, keto-, and acetyl C=O modes at the periphery of the protein molecules, which can form hydrogen bonds to suitable partners in the protein site were also analyzed with IR study. Investigation revealed the presence of keto C=O (1715–1650 cm^{-1}) and acetyl C=O group (1650 and 1620 cm^{-1} but no ester C=O group (1750–1710 cm^{-1}). An essentially symmetric and weak hydrogen bonding was also observed from C=O stretches at approximately either 1654.9241 or 1670.3547 cm^{-1}. In particular, absorptions arising from turn structures are difficult to assign, due to the different hydrogen bonding characteristics of the various types of turn. In some points, β-turns may give rise to a number of amide absorptions and a low-frequency absorption (1645 to 1630

cm^{-1}) attributed to C=O groups may be involved in hydrogen bonds which may stabilize the turn. Although a high frequency absorption (1660 to 1680 cm^{-1}) may be from C=O groups that sterically constrained and are not hydrogen bonded. It was evident from the **Figure 4.23** that a sharp shoulder at 1635.6360 cm^{-1} indicates C=O groups involved in hydrogen bonding that stabilized the turn and presence of non hydrogen bonded amide C=O group at 1670.3547 cm^{-1} (1666– 1670 cm^{-1} and antiparallel β-sheet structures (1674.2123 and 1683.8564 cm^{-1}) indicates that protein can be assigned to a high-frequency β-sheet component that arises from transition dipole coupling.

Primary amides ($-NH_2$) band near 3350 cm^{-1} (3354.2110 cm^{-1}) indicates that protein can also be assigned to a high asymmetric N-H stretch and Secondary amides have one band (-NH) near 3300 cm^{-1} (3334.9229 cm^{-1}).

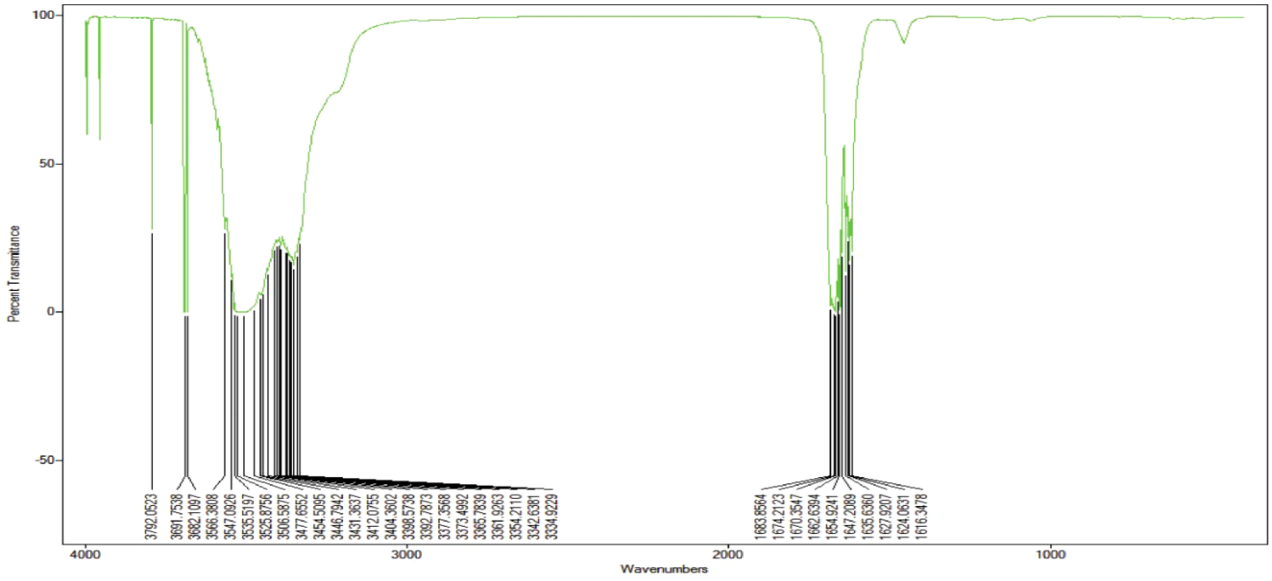

Figure 4.23 FTIR spectrum of purified Acp-N84 protein.

4.9.3 MALDI-MS study

The protein band of Acp-N84 was excised and subjected to in-gel digestion with trypsin. Proteolytic fragments were analyzed by MALDI-TOF MS as well as nano liquid chromatography mass spectrometry (Bruker Ultraflex TOF/TOF) to identify potential peptide candidates. **Figure 4.24** shows the mass spectrum of trypsin-digested peptides of Acp-N84.

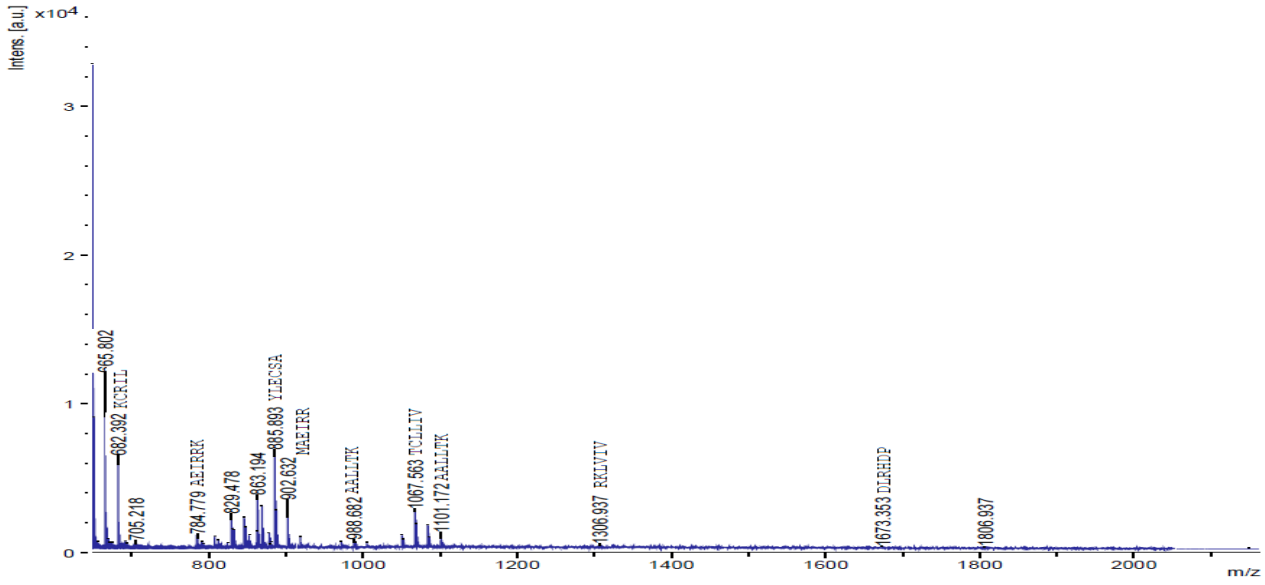

Figure 4.24 Peptide mass fingerprinting of Acp-N84 by MALDI-TOF MS.

The Mascot algorithm was employed for protein identification by peptide mass fingerprinting. This revealed a partial sequence of the examined protein. An LRHDPKTIEELT peptide fragment of a hypothetical protein from *Aspergillus giganteus* MTCC 8408 was identified. The MALDI-TOF and liquid chromatography mass spectra data revealed the potential match with putative GTP-binding protein from *Aspergillus* species, which showed a significant score of up to 92 (**Table 4.16**).

Table 4.16 Analysis of Acp-N84 by MALDI-TOF MS (results of BLAST search)

Identified protein (Accession no.)	Molecular mass (Da)	Score	Tryptic matched Peptides	Protein name
A0A017SRK7	21590	92	12	GTP-binding protein rhoA
A0A1L9W076	21590	92	12	Uncharacterized protein
A0A0U5GTW3	21736	92	12	Putative GTP-binding protein rhoA
A1CE80	21665	92	12	Rho GTPase RHO1
A0A0J5Q6F2	22530	85	12	Rho GTPase RHO1
A0A2I1CDI7	22558	85	12	Rho GTPase RHO1

There were at least 12 peptides in Acp-N84 that were homologous to putative GTP-binding protein from Aspergillus species. The matched peptide sequences of Acp-N84 were aligned based on their occurrence and subjected to an NCBI BLAST, Uni-Prot and AspGD search. The results showed 33% homology with putative GTP-binding protein from *Aspergillus calidoustus* (**Table 4.17**). The measured molecular mass of the purified Acp-N84 protein corresponded well to the calculated mass of the identified fragment MAEIRRKLVIVGDGACGKTCLLIVFSKD**LRHDPKTIEELT**KKKIGAYKTNEGVRAALLT KKKCR of this hypothetical protein.

Table 4.17 Sequence of peptides matched with the putative GTP-binding protein of *Aspergillus calidoustus* strain (gi|972235139) after Tryptic digestion of Acp-N84, analyzed by the Mascot algorithm*. Peptides are aligned by their residue numbers. Fixed modifications: carbamidomethyl (C); variable modifications: oxidation (M); sequence coverage: 33 %.

Query	Start-End	Observed	Molecular weight (expected)	Molecular weight (calculated)	Miss	Peptide sequence
58	1-7	919.3541	918.3468	918.5069	2	.MAEIRRK + Oxidation
73	8 – 27	2149.8105	2148.8032	2149.1639	1	K.LVIVGD
54	120 – 126	880.6241	879.6168	879.4563	1	K.DLRHDP
45	127 – 133	833.0534	832.0461	832.4542	0	K.TIEELT
40	149 – 155	807.4029	806.3956	806.5014	2	R.KKIGAY
30	163 – 168	675.2815	674.2742	674.3347	0	R.TNEGVR
15	177 – 182	616.1277	615.1204	615.3955	0	R.AALLTK
9	188 – 191	591.3789	590.3716	590.3322	2	K.KKCR.I

*with approximate 10-15 shots (500 counts/shot) and 8-10 independent peptides were identified.

4.10 Molecular identification

4.10.1 *in silico* investigations of Acp-N84

Based on in silico investigations, the Acp-N84 consists of 64 amino acids length mature form of pre-protein and has an observed molecular weight of 7157.62 Da and pI of 9.90. The instability index was computed to be 38.62 (ExPAsy ProtParam prediction), classified this protein as stable with half life of 30 h in-vitro (mammalian reticulocytes). Acp-N84 was hydrophilic (GRAVY = −0.2921875) in the consequence of the R/K/D/E = 5/11/3/4 amino acid ratio **(Table 4.18)**.

The confidence of three cysteines bonding residues showed the possibility of two disulfide bridges **(Figure 4.25)** between C16 and C20 and C63 (DISULFIND prediction). The SignalP1 4.1 server predicted the cleavage site of the signal sequence MAEIRRK with maximum S score (0.268) at position 4 **(Figure 4.26)** while the predicted secondary structure sequence appeared CCCCCCCEEEE**.** The PSIPRED predicted signal sequence with maximum confidence of α-helix form was EGVRAALLTKKKCR **(Figure 4.27)**.

```
         .........10.........20.........30.........40.........50.........60...
AA       MAEIRRKLVIVGDGACGKTCLLIVFSKDLRHDPKTIEELTKKKIGAYKTNEGVRAALLTKKKCR
DB_state              0   0                                                0
DB_conf               6   7                                                5
```

Figure 4.25 Prediction of disulfide bridges formation (DISULFIND)

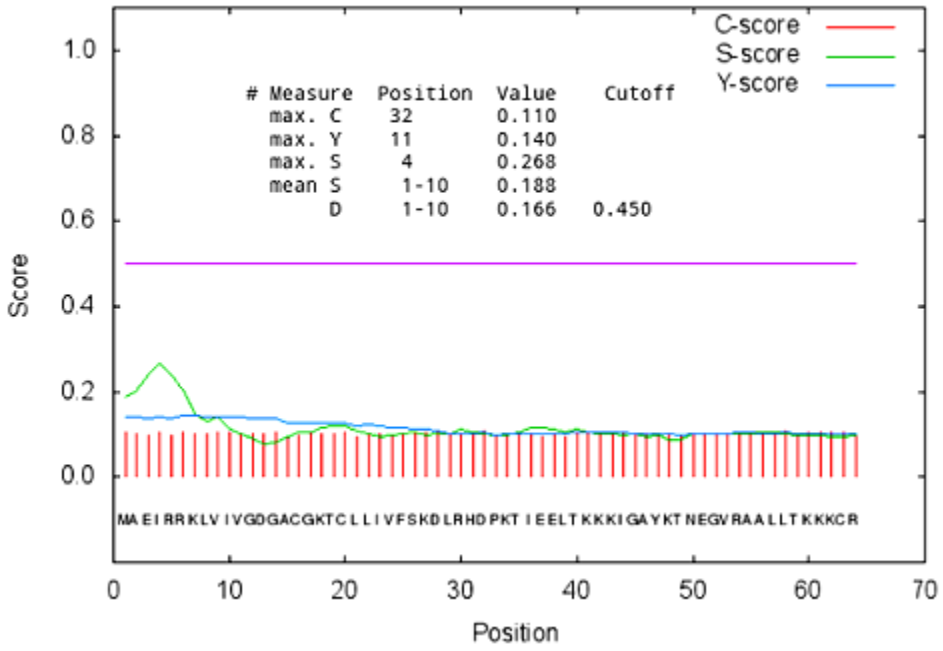

Figure 4.26 Cleavage site prediction of the signal sequence (SignalP1-4.1)

Table 4.18 Amino acid composition of Acp-N84 (ExPAsy ProtParam)

Amino acid	Residue	Composition (%)
Ala (A)	5	7.8
Arg (R)	5	7.8
Asn (N)	1	1.6
Asp (D)	3	4.7
Cys (C)	3	4.7
Gln (Q)	0	0.0
Glu (E)	4	6.2
Gly (G)	5	7.8
His (H)	1	1.6
Ile (I)	5	7.8
Leu (L)	7	10.9
Lys (K)	11	17.2
Met (M)	1	1.6
Phe (F)	1	1.6
Pro (P)	1	1.6
Ser (S)	1	1.6
Thr (T)	5	7.8
Trp (W)	0	0.0
Tyr (Y)	1	1.6
Val (V)	4	6.2
Pyl (O)	0	0.0
Sec (U)	0	0.0

Sec (U)-selenocysteine; Pyl (O)-pyrrolysine; Gln (Q)-glutamine

Figure 4.27 Protein structure predictions (PSIPRED)